Numerical approximation of the Steiner problem in dimension 2 and 3

Matthieu Bonnivard* Elie Bretin† Antoine Lemenant‡

April 10, 2018

Abstract

The aim of this work is to present some numerical computations of solutions of the Steiner Problem, based on the recent phase field approximations proposed in [12] and analyzed in [5, 4]. Our strategy consists in improving the regularity of the associated phase field solution by use of higher-order derivatives in the Cahn-Hilliard functional as in [6]. We justify the convergence of this slightly modified version of the functional, together with other technics that we employ to improve the numerical experiments. In particular, we are able to consider a large number of points in dimension 2. We finally present and justify an approximation method that is efficient in dimension 3, which is one of the major novelties of the paper.

Contents

*Université Paris-Diderot, Sorbonne Paris-Cité, Sorbonne Université, CNRS, Laboratoire Jacques-Louis Lions, F-75013 Paris (bonnivard@ljll.univ-paris-diderot.fr)

†Univ Lyon, INSA de Lyon, CNRS UMR 5208, Institut Camille Jordan 20 avenue Albert Einstein, F-69621 Villeurbanne Cedex, France (elie.bretin@insa-lyon.fr)

‡Université Paris-Diderot, Sorbonne Paris-Cité, Sorbonne Université, CNRS, Laboratoire Jacques-Louis Lions, F-75013 Paris (lemenant@ljll.univ-paris-diderot.fr)

1 Introduction

Consider a bounded and convex open set $\Omega \subset \mathbb{R}^d$. The Steiner problem consists in finding, for a given collection of points $a_0, \cdots, a_N \in \Omega$, a compact connected set $K \subset \Omega$ containing all the a_i's and having minimal length. In other words, it amounts to solving the minimization problem

$$\min\{\mathcal{H}^1(K); K \subset \Omega, \text{connected, and containing all points } a_i\}, \tag{1.1}$$

where $\mathcal{H}^1(K)$ stands for the one dimensional Hausdorff measure of K.

This very old problem, stated more than two centuries ago, is known as a (NP)-hard problem in combinatorial theory (see e.g. [11]). Finding efficient algorithms to compute an approximate solution is still an active research fieldin graph theory (see for instance [9] and references therein). We also refer to [13] for the study in a general metric space setting.

In this paper, we consider the problem from a variational point of view, based on the phase field approximation that has been recently introduced in [12] and analyzed in [5, 4] (see also [7, 8, 3] for different approaches). The model which has been proved to work in dimension 2, consists in coupling a Cahn-Hilliard type functional

$$P_\varepsilon(u) = \int_{\mathbb{R}^2} \varepsilon|\nabla u|^2 + \frac{1}{\varepsilon}V(u)dx$$

with a penalized term that forces the connectedness of the set K. Here, ε is a small parameter and V is the single-well potential defined by $V(s) = \frac{1}{4}(1-s)^2$. More precisely, the connectedness of K is enforced by penalizing the quantity

$$\sum_{i=1}^{N} \mathbf{D}(u^2; a_0, a_i), \tag{1.2}$$

where for all nonnegative Borel measurable functions $w : \Omega \to [0, \infty)$, the function $\mathbf{D}(w; a, b)$ denotes the (generalized) geodesic distance between two points $a, b \in \Omega$ relatively to w:

$$\mathbf{D}(w; a, b) := \inf_{\Gamma : a \rightsquigarrow b} \int_\Gamma w \, d\mathcal{H}^1 \in [0, +\infty]. \tag{1.3}$$

In this definition, the notation $\Gamma : a \rightsquigarrow b$ means that Γ is a rectifiable curve in Ω connecting a and b. Notice that $\mathbf{D}(w; a, b)$ makes sense for any $w \in W^{1,1}(\Omega) \cap L^\infty(\Omega)$ but one has to consider the precise representative of the Sobolev function $w \in W^{1,1}(\Omega)$ while computing the integral on curves. In this paper we shall always tacitly work with the precise representative without specify it explicitly.

Finally, the phase field approach in [12, 5, 4] relies on the minimization among $u \in 1 + H^1_0(\Omega)$ of the following functional:

$$F_\varepsilon(u) \quad := \quad P_\varepsilon(u) + \frac{1}{\lambda_\varepsilon} \sum_{i=1}^{N} \mathbf{D}(u^2 + \delta_\varepsilon; a_0, a_i). \tag{1.4}$$

It is proved in [5, Theorem 4.2] and [4, Theorem 1.2] that, in dimension 2, letting λ_ε and δ_ε go to zero as ε goes to zero, one obtains the convergence of sublevel sets of minimizers to a solution of the Steiner problem. Notice that the introduction of an additional parameter δ_ε can be interpreted as an elliptic regularization of the initial term (1.2). Intuitively, the penalizing term implies that $\sum_{i=1}^{N} \mathbf{D}(u^2; a_0, a_i) = 0$ at the limit $\varepsilon \to 0$, which shows that the set $K := \{u = 0\}$ must be path connected to all the points a_i. Moreover, the Cahn-Hilliard energy forces u to be equal to 1 in $\mathbb{R}^2 \setminus K$, and its contribution gives an approximation of $\mathcal{H}^1(K)$.

In order to handle more general Steiner problems, it is possible to replace the penalized term (1.2) by

$$\int_\Omega \mathbf{D}\big(u^2 + \delta_\varepsilon; a_0, x\big)\, d\mu, \tag{1.5}$$

where μ is a positive measure supported in Ω. In that case, the zero level set of a minimizer u of the functional $P_\varepsilon(u) + \frac{1}{\lambda_\varepsilon} \int_\Omega \mathbf{D}\big(u^2; a_0, x\big)\, d\mu$ is an approximation of the compact connected set K containing the support of μ, with minimal length, as studied in [13]. In this setting, the term (1.2) corresponds to the choice

$$\mu := \sum_{i=1}^{N} \delta_{a_i}, \tag{1.6}$$

where δ_{a_i} stands for the Dirac mass at point a_i. In this paper we assume that the measure μ is discrete, and defined by (1.6); however, the same approach could also be used for a general measure by adding weights, *i.e.* by considering an approximation of μ of the form

$$\mu := \sum_{i=1}^{N} \beta_i \delta_{a_i}. \tag{1.7}$$

For simplicity we do not pursue this approach here but focus on measures of type (1.6), corresponding to the original Steiner problem (1.1).

The aim of this paper is twofold: firstly, improve the numerical experiments by use of several regularization effects in the functional, secondly, present and justify a method that works in dimension 3 as well.

More precisely, we are interested in the derivation of an efficient numerical scheme to approximate the minimization problem

$$\min_{u \in 1 + H^1_0(\Omega)} F_\varepsilon(u), \tag{1.8}$$

where F_ε is the functional defined in (1.4). A first idea should be to compute a time-discretization of the L^2-gradient flow of $F_\varepsilon(u)$, i.e,

$$u_t = -\nabla F_\varepsilon(u).$$

However, this strategy raises some difficulties in the computation of the gradient of the geodesic terms with respect to u. Even if numerical methods have been developed to differentiate geodesics with respect

to the metric (see for instance, [2]), in practice, these computations may exhibit some anisotropy issues, or more generally, a dependence on the spatial discretization of the domain. Besides, the cost of the numerical differentiation of the geodesic distance can become prohibitive if the number of Steiner points N increases.

In order to avoid the differentiation of the geodesic distance $\mathbf{D}\big(w; a_0, a_i\big)$ with respect to the metric w, we adopt the point of view developed in [4], that consists in dissociating the minimization problem (1.8) by introducing an extra variable $\boldsymbol{\gamma} := (\gamma_i)_{1\leq i\leq N}$, where each γ_i is a Lipschitz curve joining the base point a_0 to the point a_i in Ω. Following the notation in [4], we define for any pair of distinct points $a, b \in \Omega$ the set

$$\mathcal{P}(a,b) := \Big\{\gamma \in \mathrm{Lip}([0,1]; \overline{\Omega}_0) : \gamma(0) = a \text{ and } \gamma(1) = b\Big\},$$

and introduce the admissible set

$$\mathcal{P}(a_0,\mu) := \Big\{\boldsymbol{\gamma} = (\gamma_i)_{i=1}^N : \gamma_i \in \mathcal{P}(a_0,a_i)\Big\}.$$

Let $E_\varepsilon(u,\boldsymbol{\gamma})$ be defined through

$$E_\varepsilon(u,\boldsymbol{\gamma}) := P_\varepsilon(u) + \frac{1}{\lambda_\varepsilon}\sum_{i=1}^N \int_{\Gamma(\gamma_i)} (\delta_\varepsilon + u^2)\, d\mathcal{H}^1, \tag{1.9}$$

where for each $1 \leq i \leq N$, $\Gamma(\gamma_i)$ is defined by $\Gamma(\gamma_i) = \gamma_i([0,1])$. Using Definition (1.3), the value $F_\varepsilon(u)$ can be obtained by the identity

$$F_\varepsilon(u) = \inf_{\boldsymbol{\gamma}\in\mathcal{P}(a_0,\mu)} E_\varepsilon(u,\boldsymbol{\gamma}).$$

In this framework, the minimization problem (1.8) now takes the form

$$\inf\big\{E_\varepsilon(u,\boldsymbol{\gamma}),\ u \in 1 + H_0^1(\Omega),\ \boldsymbol{\gamma} \in \mathcal{P}(a_0,\mu)\big\}. \tag{1.10}$$

This suggests to compute a minimizing sequence for F_ε by considering the following L^2-gradient flow of E_ε:

$$\begin{cases} u_t = -\nabla_u E_\varepsilon(u,\boldsymbol{\gamma}) \\ \boldsymbol{\gamma} = \mathrm{Argmin}_{\boldsymbol{\gamma}}\{E_\varepsilon(u,\boldsymbol{\gamma})\}. \end{cases}$$

Then, an approximation $(u^n,\boldsymbol{\gamma}^n)$ of the flow $(u,\boldsymbol{\gamma})$ at time $t = n\delta_t$ can be obtained by the following time-decoupled scheme:

Step 1 – Computation of $\boldsymbol{\gamma}^n$ as

$$\boldsymbol{\gamma}^n = \mathrm{Argmin}_{\boldsymbol{\gamma}\in\mathcal{P}(a_0,\mu)} E_\varepsilon(u^n,\boldsymbol{\gamma}).$$

Step 2 – Computation of the function u^{n+1} defined by $u^{n+1} = v(\delta_t)$ where v is the solution to the following PDE:

$$\begin{cases} v_t = -\nabla_u E_\varepsilon(v,\boldsymbol{\gamma}^n) \\ v(.,0) = u^n(.) \end{cases}$$

One major advantage of this approach is that v can be computed without requiring the differentiation of the geodesic distance with respect to the metric, which is known to be a very expensive procedure.

However, two major difficulties remain in the computation of step 2. The first one results from the lack of regularity of the solution u, which is only $C^{0,\alpha}$ for all $\alpha \in (0,1)$. As a result, u is not smooth enough

to be discretized in space with a sufficient precision, which globally reduces the rate of convergence of the numerical scheme. The second difficulty concerns the geodesic term R_ε, defined by

$$R_\varepsilon(u) = \sum_{i=1}^{N} \int_{\Gamma(\gamma_i)} (\delta_\varepsilon + u^2)\, d\mathcal{H}^1. \tag{1.11}$$

Indeed, its differential with respect to u is in general a measure, which raises some instability issues if one uses a classical time discretization scheme for the computation of v.

In this paper, we explain how we can slightly modify the previous phase field model to improve the regularity of the solution u, and to facilitate the derivation of a simple unconditionnally-stable scheme.

1.1 Modified phase field models

In order to enhance the regularity of the phase field function u, the idea consists in considering a higher-order Edge penalization in the Cahn-Hilliard functional as in the recent work [6]. This amounts to using a second-order Cahn-Hilliard type energy to approximate $\mathcal{H}^1(K)$, of the form

$$\tilde{P}_\varepsilon(u) = \int_{\mathbb{R}^2} \varepsilon^3 |\Delta u|^2 + \frac{1}{\varepsilon} V(u) dx.$$

These higher order energies are convenient to regularize the profiles of the minimizers near the singular sets, and therefore, to improve the precision of the spatial discretization and the performances of the numerical methods.

Another remarkable property of the second-order approximations of the length is that they can be used in dimension 3 as well. In that case, for instance, one can consider the modified energy

$$\tilde{P}_\varepsilon(u) = \int_{\mathbb{R}^3} \varepsilon^2 |\Delta u|^2 + \frac{1}{\varepsilon^2} V(u) dx.$$

In this expression, the usual gradient term has been replaced by a Laplacian which, as opposed to the gradient, is able to detect 1-dimensional objects in $\mathbb{R}^3$. In Section 2.2, we will give some evidence about the Γ-convergence of this functional to the length, based on arguments that are rigorously justified in dimension 2, and extended to dimension 3 provided that some reasonable estimate on the optimal radial profile holds true (2.26).

About the second point, recall that the numerical computation of the solution v to the equation

$$v_t = -\nabla_u E_\varepsilon(v, \boldsymbol{\gamma}^n) = 2\varepsilon \Delta v - \frac{1}{\varepsilon} V'(v) - \frac{2}{\lambda_\varepsilon} \left[\sum_{i=1}^{N} \mathcal{H}^1|_{\Gamma(\gamma_i)} \right] v,$$

raises some numerical stability issues, due to the presence of singular measures $\mathcal{H}^1|_{\Gamma(\gamma_i)}$. A natural way of regularizing these measures is to consider the convolution with a kernel $\rho_{\varepsilon^\alpha}$ of size ε^α, *i.e.* $\rho_\varepsilon = \frac{1}{\varepsilon^2}\rho(\cdot/\varepsilon)$. This leads to the regularized geodesic term

$$\tilde{R}_\varepsilon(u, \boldsymbol{\gamma}) = \frac{1}{\lambda_\varepsilon} \int_\Omega \left[\sum_{i=1}^{N} (\rho_{\varepsilon^\alpha} * \mathcal{H}^1|_{\Gamma(\gamma_i)}) \right] (\delta_\varepsilon + u^2)\, dx.$$

In the rest of the paper, we will denote by $\omega^\varepsilon[\boldsymbol{\gamma}]$ the function

$$\omega^\varepsilon[\boldsymbol{\gamma}] = \sum_{i=1}^{N} (\rho_{\varepsilon^\alpha} * \mathcal{H}^1|_{\Gamma(\gamma_i)}). \tag{1.12}$$

As the minimizer u_ε of $E_\varepsilon(u, \boldsymbol{\gamma})$ is expected to take the form

$$u_\varepsilon(x) = q(\mathrm{dist}(x, \Gamma(\boldsymbol{\gamma}))/\varepsilon),$$

where q is a phase field profile (which is explicit and depends only on the single-well potential V), we see that α should satisfies $\alpha > 1$ to reduce the effect of this regularization when $\varepsilon \to 0$. A more thorough discussion about this regularized term will be done in Section 2.4.

Moreover, in practice and in our numerical experiments, we can observe (see for instance figure 8) that the width of the sublevel sets of u can vary along the support of $\boldsymbol{\gamma}$. More precisely, the width of these sets increases around points $x \in \boldsymbol{\gamma}$ that are crossed by multiple geodesics γ_i. This results from the use of a penalization term $\omega^\varepsilon[\boldsymbol{\gamma}]$, whose weight is not uniform along the support of $\boldsymbol{\gamma}$. Even if this issue may not be crucial for a small number of points a_i (less than 10 for instance), it makes the method inefficient for a large number of attachment points, since the geodesics may not be precisely detected by the phase field u.

Hence, we propose to reduce these adverse effects by considering the weight

$$\omega^\varepsilon_{\max}[\boldsymbol{\gamma}] = \mathrm{Max}_{i=1}^N \left\{ \rho_{\varepsilon^\alpha} * \mathcal{H}^1|_{\Gamma(\gamma_i)} \right\},$$

and the associated geodesic term

$$\tilde{R}_{\varepsilon,\max}(u, \boldsymbol{\gamma}) = \frac{1}{\lambda_\varepsilon} \int_\Omega \omega^\varepsilon_{\max}[\boldsymbol{\gamma}](\delta_\varepsilon + u^2)\, dx.$$

1.2 Outline of this paper

Section 2 recalls some results from [5, 4] and gives mathematical justifications of the different modified phase field models that we propose. This section is purely theoretical. The first result contains a full Γ-convergence proof in dimension two (Proposition 2.4) inspired by the work in [6]. Its extension to dimension three requires a rather technical study of the corresponding 1D-profile (or more precisely, radial profile). The main result of this section is the existence of a radial profile for the 3D energy as stated in Lemma 2.10. We then discuss the proof of Γ-convergence in dimension three, which relies on certain estimates on the unknown radial profile, that are justified by some numerical evidence. In the last Section 2.4, we compare the functional with its regularized version, that involves a convolution kernel in the geodesic term.

Section 3 provides numerical experiments and compares the different approaches to approximate the Steiner optimization problem. In particular, we present some 2D examples with a large number of points (up to 100 points). We also show satisfactory experiments in 3D. To our best knowledge, it would be the first time that the Steiner problem is solved in space dimension three, by use of a phase-field method.

1.3 Acknowledgements

We would like to express our gratitude to Vincent Millot for his precious comments and ideas, and many fruitful discussions relative to this work. This work has been supported by the PGMO project COCA from the Hadamard fundation.

2 Theoretical analysis of the various phase field models

In this section we justify our numerical method by recalling some convergence results from [4]. We then discuss the incidence of small variants of the functional introduced in [4], that we used in practice. In

particular, a full Γ-convergence result is proved for a second-order functional in dimension 2, and its potential extension to dimension 3 is discussed.

2.1 Main results from [4]

In this section we collect some useful results contained in [4] concerning the minimization problem (1.8) and its convergence as $\varepsilon \to 0$. We keep the same notation as in the introduction. We assume that $\Omega \subset \mathbb{R}^2$ is convex and $\{a_i\}_{i=1,\dots,N} \subset \Omega$ are given points. We also, as before, denote by $\mu := \sum_{i=1}^N \delta_{a_i}$.

Notice that in [4], precise estimates are given, with constants depending explicitely on parameters $\varepsilon, \delta_\varepsilon, \lambda_\varepsilon$. Since we are mainly concerned with the asymptotic behaviour of the minimizers when $\varepsilon \to 0$, we will assume that all these parameters are small, *i.e.* $\varepsilon, \delta_\varepsilon, \lambda_\varepsilon << 1$. As a consequence, some statements will be simplified.

Minimization problem with prescribed curves

For a given set of curves $\boldsymbol{\gamma} \in \mathcal{P}(a_0, \mu)$, we consider the functional $E_\varepsilon(\cdot, \boldsymbol{\gamma}) : H^1(\Omega) \to [0, +\infty]$ already defined in (1.9) by

$$E_\varepsilon(u, \boldsymbol{\gamma}) := \varepsilon \int_\Omega |\nabla u|^2 \, dx + \frac{1}{4\varepsilon} \int_\Omega (u-1)^2 \, dx + \frac{1}{\lambda_\varepsilon} \sum_{i=1}^N \int_{\Gamma(\gamma_i)} (\delta_\varepsilon + u^2) \, d\mathcal{H}^1, \tag{2.1}$$

and we introduce the minimization problem

$$\min_{u \in 1 + H_0^1(\Omega)} E_\varepsilon(u, \boldsymbol{\gamma}). \tag{2.2}$$

It is proved in [4] that problem (2.2) has a unique solution, provided that $\boldsymbol{\gamma}$ satisfies a mild regularity constraint, that can be expressed in terms of Ahlfors regularity. Let us recall that the Ahlfors constant $\mathbf{Al}(K)$ of a closed set $K \subset \mathbb{R}^2$ is defined by

$$\mathbf{Al}(K) := \sup \left\{ \frac{\mathcal{H}^1(K \cap B(x,r))}{r} : r > 0 \,,\ x \in K \right\}.$$

For any $\Lambda \geq 2$, we introduce the subset $\mathcal{P}_\Lambda(a_0, \mu)$ of $\mathcal{P}(a_0, \mu)$ defined by

$$\mathcal{P}_\Lambda(a_0, \mu) := \Big\{ \boldsymbol{\gamma} \in \mathcal{P}(a_0, \mu) : \mathbf{Al}\big(\Gamma(\gamma_i)\big) \leq \Lambda \text{ for each } i \Big\}.$$

This definition is motivated by the fact that whenever $\boldsymbol{\gamma} \in \mathcal{P}_\Lambda(a_0, \mu)$, the bilinear form

$$(u, v) \in H^1(\Omega) \times H^1(\Omega) \mapsto \sum_{i=1}^N \int_{\Gamma(\gamma_i)} uv \, d\mathcal{H}^1 \tag{2.3}$$

is continuous. It follows that $E_\varepsilon(u, \boldsymbol{\gamma})$ is finite for every $u \in 1 + H_0^1(\Omega)$. Besides, the mapping $v \in H^1(\Omega) \mapsto E_\varepsilon(v, \boldsymbol{\gamma})$ is lower semi-continuous with respect to the weak $H^1(\Omega)$ convergence, and by strict convexity of this functional, there holds following result.

Theorem 2.1. ([4, Theorem 2.3 and Proposition 2.10]) *Given $\boldsymbol{\gamma} \in \mathcal{P}_\Lambda(a_0, \mu)$, problem (2.2) admits a unique solution $u_{\boldsymbol{\gamma}}$, which satisfies the Euler-Lagrange equation*

$$\begin{cases} -\varepsilon^2 \Delta u_{\boldsymbol{\gamma}} = \dfrac{1}{4}(1 - u_{\boldsymbol{\gamma}}) - \dfrac{\varepsilon}{\lambda_\varepsilon} u_{\boldsymbol{\gamma}} \mathcal{H}^1|_{\Gamma(\boldsymbol{\gamma})} & \text{in } H^{-1}(\Omega)\,, \\ u_{\boldsymbol{\gamma}} = 1 & \text{on } \partial\Omega. \end{cases} \tag{2.4}$$

Moreover, $u_{\boldsymbol{\gamma}} \in C^{0,\alpha}(\Omega)$ for every $\alpha \in (0,1)$ with the estimate

$$\|u_\varepsilon\|_{C^{0,\alpha}} \leq C_\alpha \frac{1}{\varepsilon^\alpha \delta_\varepsilon \lambda_\varepsilon}. \tag{2.5}$$

Thanks to the Hölder regularity of $u_{\boldsymbol{\gamma}}$, it is then easily possible to minimize E_ε in the $\boldsymbol{\gamma}$ variable with u fixed in $C^{0,\alpha}$, which justifies theorically the algorithm described in the introduction.

Existence and uniqueness of the minimizer for F_ε

By the very definition of F_ε, the functional E_ε relates to F_ε through the formula

$$F_\varepsilon(u) = \inf_{\boldsymbol{\gamma} \in \mathcal{P}(a_0,\mu)} E_\varepsilon(u, \boldsymbol{\gamma}). \tag{2.6}$$

Hence, the existence result for F_ε follows from the existence of a minimizing pair $(u_\varepsilon, \boldsymbol{\gamma}_\varepsilon)$ for E_ε, that we state as a preliminary result.

Theorem 2.2. [4, Theorem 2.12] *The functional E_ε admits at least one minimizing pair $(u_\varepsilon, \boldsymbol{\gamma}_\varepsilon)$ in $(1 + H_0^1(\Omega)) \times \mathcal{P}(a_0, \mu)$. In addition, for any such minimizer, $\boldsymbol{\gamma}_\varepsilon$ belongs to $\mathcal{P}_{\Lambda_\varepsilon}(a_0, \mu)$, with $\Lambda_\varepsilon = 4/\delta_\varepsilon$ and u_ε is the minimizer of problem (2.2) with $\boldsymbol{\gamma} = \boldsymbol{\gamma}_\varepsilon$.*

From Theorem 2.2 we can deduce the following.

Theorem 2.3. [4, Corollary 2.13] *The functional F_ε admits at least one minimizer u_ε in $1 + H_0^1(\Omega) \cap L^\infty(\Omega)$. In addition, any such minimizer belongs to $W^{1,p}(\Omega)$ for every $p < \infty$. In particular, $u_\varepsilon \in C^{0,\alpha}(\Omega)$ for every $\alpha \in (0,1)$ with the estimate*

$$\|u_\varepsilon\|_{C^{0,\alpha}} \leq C_\alpha \frac{1}{\varepsilon^\alpha \delta_\varepsilon \lambda_\varepsilon}. \tag{2.7}$$

Moreover, there exists $\boldsymbol{\gamma}_\varepsilon \in \mathcal{P}(a_0, \mu)$ such that $(u_\varepsilon, \boldsymbol{\gamma}_\varepsilon)$ is a minimizing pair for E_ε in $(1 + H_0^1(\Omega)) \times \mathcal{P}(a_0, \mu)$. In addition, $\boldsymbol{\gamma}_\varepsilon$ belongs to $\mathcal{P}_{\Lambda_\varepsilon}(a_0, \mu)$, with $\Lambda_\varepsilon = 4/\delta_\varepsilon$ and u_ε is the minimizer of problem (2.2) with $\boldsymbol{\gamma} = \boldsymbol{\gamma}_\varepsilon$.

2.2 Analysis of the second-order functional in dimension 2

In this section we discuss the incidence of replacing ∇u by Δu in the functional, which helps in getting better numerical results by regularizing the profile of the phase field u in the transition region, near the curves. To this aim, we look at the Γ-convergence of the higher order functional in dimension 2,

$$G_\varepsilon(u) := \int_\Omega \varepsilon^{5-d} |\Delta u|^2 + \frac{(1-u)^2}{\varepsilon^{d-1}}\, dx + \frac{1}{\lambda_\varepsilon} \int_K (u^2 + \delta_\varepsilon) d\mathcal{H}^1,$$

that we used in our numerical experiments in dimension $d = 2$ and $d = 3$.

We first state a result in dimension 2, which provides the Γ-convergence in the simple case when K is a segment. Our proof is strongly inspired by the Γ-convergence result in [6]. This is why we use in this section the potential $V(u) = (1-u)^2$ instead of $V(u) = \frac{1}{4}(1-u)^2$ as it is done in the rest of the paper.

Proposition 2.4. *(Γ-convergence for K fixed). Let $d = 2$ and K be a segment. We assume that $\delta_\varepsilon/\lambda_\epsilon \to 0$. Then, in the L^1 topology, there holds*

$$\Gamma - \lim G_\varepsilon = \begin{cases} 2\sqrt{2}\mathcal{H}^1(K) & \text{if } u = 1 \text{ a.e.} \\ +\infty & \text{otherwise.} \end{cases}$$

Remark 2.5. *From Proposition 2.4 it would be easy to conjecture that the same holds true for any 1-rectifiable set K. Indeed, a simple variant of our argument would probably work for any polygonal line K, and then passing from polygonal lines to any rectifiable set is a matter of technical details, that we decided to avoid in this presentation.*

Remark 2.6. *We expect the same result to hold for $d = 3$, but the proof is more complicated, since it involves sets of co-dimension 2 in $\mathbb{R}^3$. We will discuss this extension in the next Section 2.3.*

As usual in Γ-convergence, we divide the proof in two parts, corresponding to the liming and limsup inequalities. Before doing so, we analyse the optimal 1D-profiles.

2.2.1 One-dimensional optimal profile analysis

In this section we are interested in the 1D optimal profiles that will be used in the Γ-limsup inequality. We first explain the heuristic before making precise computations. The idea is to analyse, in the case where K is a line in $\mathbb{R}^2$, what would be a minimizer u of the form

$$u(x) = v\left(dist(x, K)\right), \tag{2.8}$$

where $v : \mathbb{R} \to \mathbb{R}$.

We assume for instance that K is the line $\mathbb{R}\mathbf{e}_1$. We then notice that the function u of the form (2.8) is constant in the $\mathbf{e}_1$ direction, and we are thus interested in the energy of the $\mathbf{e}_1^\perp$ components. In $\mathbb{R}^2$, it reduces to the simple 1D-energy

$$\int_{\mathbb{R}} \varepsilon^3 (v''(r))^2 + \frac{1}{\varepsilon}(1 - v(r))^2 \, dr + \frac{1}{\varepsilon^\gamma}\left(v^2(0) + \delta_\varepsilon\right),$$

which motivates the definition of the following variational problem, after rescaling $v(r)$ by $v(\varepsilon r)$:

$$m_{2D} := \begin{cases} \min\limits_v E_{2D} := \displaystyle\int_0^{+\infty} \left(v''(r)\right)^2 + \left(1 - v(r)\right)^2 dr, \\ v \in H^2_{loc}(0, +\infty)\ ,\ v(0) = 0\ ,\ v'(0) = 0\ ,\ \lim\limits_{r \to +\infty} v(r) = 1 \end{cases} \tag{2.9}$$

We added condition $v'(0) = 0$ because we have in mind an even profile on $\mathbb{R}$. The above minimization problem can be solved explicitly using the associated Euler equation, as in [6, (3.3)], and the solution is given by

$$\varphi(r) = 1 - \sqrt{2} e^{-\frac{r}{\sqrt{2}}} \sin\left(\frac{r}{\sqrt{2}} + \frac{\pi}{4}\right).$$

By a computation we deduce that

$$m_{2D} = \sqrt{2}, \quad r \geq 0.$$

2.2.2 Proof of Γ-liminf for $d = 2$.

To prove the Γ-liminf inequality, we first prove the following one-dimensional liminf inequality.

Lemma 2.7 (One-dimensional liminf inequality for the two-dimensional profile)**.** *Let $T > 0$ be fixed. Let v_ε be any $C^1([-T, T])$ sequence such that $v_\varepsilon \to 1$ in $L^1([-T, T])$, and $v_\varepsilon(0) \to 0$. Then*

$$\liminf_\varepsilon \int_{-T}^{T} \varepsilon^3 \left(v_\varepsilon''\right)^2 + \frac{1}{\varepsilon}(1 - v_\varepsilon)^2 \, dt \geq 2 m_{2D}. \tag{2.10}$$

Proof. This is essentially the core of the proof of the liminf in [6], but for the reader's convenience we rewrite some details in our particular context. We may assume that the above liminf is finite and that v_ε is a sequence that realizes the liminf. Let ε_0 be fixed. Then there exists a constant $C > 0$ such that

$$\sup_{0<\varepsilon<\varepsilon_0} \int_{-T}^{T} (\varepsilon^3 (v_\varepsilon'')^2 + \frac{1}{\varepsilon}(1-v_\varepsilon)^2)\, dt \leq C,$$

which implies that for any $0 < \varepsilon < \varepsilon_0$,

$$\mathcal{L}^1(\{t \in [-T,T] \text{ s.t. } (1-v_\varepsilon)^2 > \sqrt{\varepsilon}\}) \leq \frac{1}{\sqrt{\varepsilon}} \int_0^T (1-v_\varepsilon)^2 dt \leq C\sqrt{\varepsilon}.$$

We deduce that there exist two sequences $s_\varepsilon^+ \in [0,T]$ and $s_\varepsilon^- \in [-T,0]$ such that

$$\lim_{\varepsilon\to 1} v_\varepsilon(s_\varepsilon^\pm) = 1.$$

Moreover, by Gagliardo-Nirenberg interpolation inequality (see for instance [6, Proposition 2.1]), there exists $c_0 > 0$ such that for any $0 < \varepsilon < \varepsilon_0$,

$$c_0\varepsilon \int_{-T}^{T} (v_\varepsilon')^2 dt \leq \frac{1}{\varepsilon}\int_{-T}^{T} (1-v_\varepsilon)^2 dt + \varepsilon^3 \int_{-T}^{T} (v_\varepsilon'')^2 dt. \tag{2.11}$$

Combining the above estimate with Hölder inequality, we obtain the existence of a constant $C > 0$ such that

$$\int_{-T}^{T} \varepsilon |v_\varepsilon'| dt \leq C\sqrt{\varepsilon} \quad \forall \varepsilon \in (0, \varepsilon_0).$$

Hence, up to a subsequence, $\varepsilon v_\varepsilon'$ converges to 0 a.e. in $(-T,T)$, and without loss of generality, we can assume that

$$\lim_{\varepsilon\to 0} \varepsilon v_\varepsilon'(s_\varepsilon^\pm) = 0.$$

Remember that we also have $\lim_{\varepsilon\to 0} v_\varepsilon(0) = 0$. Let t_ε be a minimizer of v_ε on the interval $[s_\varepsilon^-, s_\varepsilon^+]$. For ε small, we can assume $s_\varepsilon^- < t_\varepsilon < s_\varepsilon^+$, and by minimality, there holds

$$\lim_{\varepsilon\to 0} v_\varepsilon(t_\varepsilon) = 0, \quad \text{and moreover} \quad v_\varepsilon'(t_\varepsilon) = 0 \quad \text{for any } \varepsilon.$$

To estimate by below the integral $\int_{-T}^{T} (\varepsilon^3 (v_\varepsilon'')^2 + \frac{1}{\varepsilon}(1-v_\varepsilon)^2)\, dt$, we first consider the contribution of interval $[t_\varepsilon, T]$; the contribution of $[-T, t_\varepsilon]$ will be treated similarly. Let us introduce the rescaled function $w_\varepsilon(z) := v_\varepsilon(\varepsilon y + t_\varepsilon)$. Using the change of variable $r = \frac{t-t_\varepsilon}{\varepsilon}$, we get

$$\int_{t_\varepsilon}^{T} (\varepsilon^3 (v_\varepsilon'')^2 + \frac{1}{\varepsilon}(1-v_\varepsilon)^2)\, dt = \int_0^{(T-t_\varepsilon)/\varepsilon} ((w_\varepsilon'')^2 + (1-w_\varepsilon)^2)\, dr. \tag{2.12}$$

Notice that the previous properties established for v_ε now read

$$\lim_{\varepsilon\to+\infty} w_\varepsilon(0) = 0, \quad w_\varepsilon'(0) = 0 \text{ for any } \varepsilon, \quad \lim_{\varepsilon\to+\infty} w_\varepsilon\left(\frac{s_\varepsilon^+ - t_\varepsilon}{\varepsilon}\right) = 1, \quad \lim_{\varepsilon\to+\infty} w_\varepsilon'\left(\frac{s_\varepsilon^+ - t_\varepsilon}{\varepsilon}\right) = 0. \tag{2.13}$$

In order to estimate the right-hand side in (2.12), we use the construction proposed in [6] of an admissible test function $\tilde{w}_\varepsilon$ for the following minimisation problem:

$$\min\Big\{ \int_0^{+\infty} ((w''(r))^2 + (1-w(r))^2)\, dr, \\ w \in H^2_{loc}(0,+\infty)\ ,\ w(0) = v_\varepsilon(t_\varepsilon)\ ,\ w'(0) = 0\ ,\ \lim_{r\to+\infty} w(r) = 1\Big\}. \tag{2.14}$$

This problem is a slight variant of the minimisation problem (2.9) defining m_{2D}, and as stated in [6, Remark 1], the corresponding minimum is given by $\sqrt{2}\,(v_\varepsilon(t_\varepsilon)-1)^2$.

Using properties (2.13), it is possible to construct for any $\eta > 0$ a smooth function $\tilde{w}_\varepsilon$ defined on $(0,+\infty)$, that coincides with w_ε on $[0,(s_\varepsilon^+ - t_\varepsilon)/\varepsilon]$, is equal to 1 for $r \geq (s_\varepsilon^+ - t_\varepsilon)/\varepsilon + 1$, and such that

$$\int_0^{(s_\varepsilon^+ - t_\varepsilon)/\varepsilon} ((w_\varepsilon'')^2 + (1-w_\varepsilon)^2)\, dr \geq \int_0^{+\infty} ((\tilde{w}_\varepsilon'')^2 + (1-\tilde{w}_\varepsilon)^2)\, dr - \eta.$$

Let P_ε be the unique polynomial of degree less or equal to 3 satisfying

$$P_\varepsilon(0) = w_\varepsilon\left(\frac{s_\varepsilon^+ - t_\varepsilon}{\varepsilon}\right), \quad P_\varepsilon'(0) = w_\varepsilon'\left(\frac{s_\varepsilon^+ - t_\varepsilon}{\varepsilon}\right), \quad P_\varepsilon(1) = 1, \quad P_\varepsilon'(1) = 0.$$

For $r \geq 0$, we define $\tilde{w}_\varepsilon(r)$ by

$$\tilde{w}_\varepsilon(r) = \begin{cases} w_\varepsilon(z) & \text{if} \quad 0 \leq r \leq \frac{s_\varepsilon^+ - t_\varepsilon}{\varepsilon}, \\ P_\varepsilon\left(r - \frac{s_\varepsilon^+ - t_\varepsilon}{\varepsilon}\right) & \text{if} \quad \frac{s_\varepsilon^+ - t_\varepsilon}{\varepsilon} \leq r \leq \frac{s_\varepsilon^+ - t_\varepsilon}{\varepsilon} + 1, \\ 1 & \text{if} \quad r \geq \frac{s_\varepsilon^+ - t_\varepsilon}{\varepsilon} + 1. \end{cases}$$

Using the change of variables $z = r - \frac{s_\varepsilon^+ - t_\varepsilon}{\varepsilon}$ in the interval $[\frac{s_\varepsilon^+ - t_\varepsilon}{\varepsilon}, \frac{s_\varepsilon^+ - t_\varepsilon}{\varepsilon} + 1]$, we obtain

$$\int_0^{+\infty} ((\tilde{w}_\varepsilon'')^2 + (1-\tilde{w}_\varepsilon)^2)\, dr = \int_0^{(s_\varepsilon^+ - t_\varepsilon)/\varepsilon} ((w_\varepsilon'')^2 + (1-w_\varepsilon)^2)\, dr + \int_0^1 ((P_\varepsilon'')^2 + (1-P_\varepsilon)^2)\, dz.$$

Computing the interpolation polynomial P_ε explicitely, and using the two last limits in (2.13), one can easily see that when ε goes to zero, P_ε converges to 1 in $C^2([0,1])$. Since $\tilde{w}_\varepsilon$ is an admissible test function for problem (2.14), for any $\eta > 0$, there holds for ε small enough

$$\begin{aligned} \int_0^{(s_\varepsilon^+ - t_\varepsilon)/\varepsilon} ((w_\varepsilon'')^2 + (1-w_\varepsilon)^2)\, dr &\geq \int_0^{+\infty} ((\tilde{w}_\varepsilon'')^2 + (1-\tilde{w}_\varepsilon)^2)\, dr - \eta \\ &\geq \sqrt{2}\,(v_\varepsilon(t_\varepsilon)-1)^2 - \eta. \end{aligned}$$

Going back to relation (2.12), and applying a similar argument on interval $[-T, t_\varepsilon]$, we obtain that

$$\int_{-T}^{T} (\varepsilon^3\,(v_\varepsilon'')^2 + \frac{1}{\varepsilon}(1-v_\varepsilon)^2)\, dt \geq 2\sqrt{2}\,(v_\varepsilon(t_\varepsilon)-1)^2 - 2\eta.$$

Passing to the $\liminf$ in ε and letting η go to zero yields the desired result. □

Proposition 2.8 (Γ-liminf inequality, $d = 2$)**.** *Assume that $d = 2$, $K \subset \Omega$ is a segment. Then, for any sequence φ_ε converging to a function φ in $L^1(\Omega)$, there holds*

$$2\sqrt{2}\mathcal{H}^1(K) \leq \liminf_{\varepsilon\to 0} G_\varepsilon(\varphi_\varepsilon).$$

Proof. We consider a sequence φ_ε converging to a function φ in $L^1(\Omega)$. Without loss of generality, we can assume that $K = [0,\ell] \times \{0\}$ with $\ell := \mathcal{H}^1(K)$, and denote by T a positive number such that $\inf\{dist(x,\partial\Omega)\ ;\ x \in K\} \geq T$. We also assume that $\liminf_{\varepsilon\to 0} G_\varepsilon(\varphi_\varepsilon) < +\infty$, and even

$$\sup_{\varepsilon\to 0} G_\varepsilon(\varphi_\varepsilon) \leq C < +\infty.$$

But this implies

$$\int_\Omega (1-\varphi_\varepsilon)^2 \leq C\varepsilon,$$

and since Ω is bounded, $\varphi_\varepsilon \to 1$ in $L^1(\Omega)$; hence $\varphi = 1$ a.e. in Ω. In the sequel we will still index by ε a subsequence of ε. From the fact that

$$\int_K \varphi_\varepsilon^2 \, d\mathcal{H}^1 \leq C\lambda_\varepsilon \underset{\varepsilon\to 0}{\longrightarrow} 0,$$

we can extract a subsequence, not relabeled, such that $\varphi_\varepsilon \to 0$ $\mathcal{H}^1$-a.e. on K. On the other hand, by Fatou lemma we get

$$\begin{aligned}
\liminf_{\varepsilon\to 0} G_\varepsilon(\varphi_\varepsilon) &\geq \liminf_{\varepsilon\to 0} \int_\Omega \varepsilon^3 |\Delta\varphi_\varepsilon|^2 + \frac{1}{\varepsilon}(1-\varphi_\varepsilon)^2 \\
&\geq \int_0^\ell \liminf_{\varepsilon\to 0} \left(\int_{-T}^T \varepsilon^3 \left|\partial_{x_2}^2 \varphi_\varepsilon\right|^2 + \frac{1}{\varepsilon}(1-\varphi_\varepsilon)^2 \, dx_2 \right) dx_1. \qquad (2.15)
\end{aligned}$$

As a result, we are reduced to check the following one dimensional liminf inequality:

$$\liminf_{\varepsilon\to 0} \int_{-T}^T (\varepsilon^3 |v_\varepsilon''|^2 + \frac{1}{\varepsilon}(1-v_\varepsilon)^2) \, dt \geq 2m_{2D}, \qquad (2.16)$$

for any sequence of functions $v_\varepsilon : [-T,T] \to \mathbb{R}$ that satisfies $v_\varepsilon \to 1$ in $L^1([-T,T])$, $v_\varepsilon \in C^1([-T,T])$ for all ε (because $H^2(-T,T) \subset C^1([-T,T])$) and $v_\varepsilon(0) \to 0$.

The proof is then concluded by applying the 1D-case Lemma 2.7. □

2.2.3 Proof of Γ-limsup for $d = 2$

We are now ready to conclude the demonstration of our Γ-convergence result by proving the limsup inequality.

Proposition 2.9 (Γ-limsup inequality)**.** *Assume that $d = 2$, $\Omega \subset \mathbb{R}^2$ is open and bounded, and $K \subset \Omega$ is a segment. Assume also that $\delta_\varepsilon/\lambda_\varepsilon \to 0$. Then there exists a sequence $\varphi_\varepsilon \in H^2(\Omega)$ such that $\varphi_\varepsilon = 0$ on K, $\varphi_\varepsilon \to 1$ on $\partial\Omega$ and*

$$\limsup_\varepsilon G_\varepsilon(\varphi_\varepsilon) \leq 2\sqrt{2}\,\mathcal{H}^1(K).$$

Proof. We follow a standard construction in Allen-Cahn theory, defining φ_ε by

$$\varphi_\varepsilon(x) = v\left(\frac{dist(x,K)}{\varepsilon}\right), \quad x \in \Omega,$$

where v is the solution of problem (2.9) that defines m_{2D}. Notice that $\varphi_\varepsilon = 0$ on K, thus

$$\frac{1}{\varepsilon^\gamma}\int_K (\varphi_\varepsilon^2 + \delta_\varepsilon) d\mathcal{H}^1 \leq \frac{\delta_\varepsilon}{\lambda_\varepsilon}\mathcal{H}^1(K),$$

which goes to zero since $\lim_{\varepsilon\to 0}\delta_\varepsilon/\lambda_\varepsilon = 0$.

Consequently, the most delicate part to handle in G_ε is the volumic integral over Ω. By the formula

$$\Delta(v\circ f) = (v''\circ f)|\nabla f|^2 + (v'\circ f)\Delta f,$$

we get the general identity

$$|\Delta\varphi_\varepsilon|^2 = \left|\frac{1}{\varepsilon^2}v''\Big(\frac{dist(x,K)}{\varepsilon}\Big) + \frac{1}{\varepsilon}v'\Big(\frac{dist(x,K)}{\varepsilon}\Big)\Delta dist(x,K)\right|^2. \tag{2.17}$$

We assume for simplicity that $K = [0,\ell]\times\{0\}$. We divide Ω in two parts,

$$\begin{aligned}\Omega_1 &:= \Omega\cap\{(x_1,x_2)\ :\ x_1\in[0,1]\},\\ \Omega_0 &:= \Omega\setminus\Omega_1.\end{aligned}$$

We compute the energy in Ω_1 and Ω_0 separately, starting with Ω_1. We notice that in this region, $\Delta dist(x,K) = 0$. Therefore, using (2.17), and denoting by $T := diam(\Omega)$, we obtain

$$\begin{aligned}\int_{\Omega_1}(\varepsilon^3|\Delta\varphi_\varepsilon|^2 + \frac{(1-\varphi_\varepsilon)^2}{\varepsilon})\,dx \quad &\le \quad \int_0^\ell\int_{-T}^T\left(\varepsilon^3|\Delta\varphi_\varepsilon|^2 + \frac{(1-\varphi_\varepsilon)^2}{\varepsilon}\right)dx_2\,dx_1\\ &= \quad 2\int_0^\ell\int_0^T\left(\frac{1}{\varepsilon}\left(v''(x_2/\varepsilon)\right)^2 + \frac{(1-v\left(\frac{x_2}{\varepsilon}\right))^2}{\varepsilon}\right)dx_2\,dx_1\\ &= \quad 2\ell\int_0^T\left(\frac{1}{\varepsilon}\left(v''\left(\frac{x_2}{\varepsilon}\right)\right)^2 + \frac{(1-v(x_2/\varepsilon))^2}{\varepsilon}\right)dx_2\\ &= \quad 2\ell\int_0^{T/\varepsilon}\left(\left(v''(t)\right)^2 + (1-v(t))^2\right)dt\\ &\longrightarrow_{\varepsilon\to 0} \quad 2\ell m_{2D},\end{aligned}$$

which proves that

$$\limsup_{\varepsilon\to 0}\int_{\Omega_1}\varepsilon^3|\Delta\varphi_\varepsilon|^2 + \frac{(1-\varphi_\varepsilon)^2}{\varepsilon}\,dx \le 2\ell m_{2D}.$$

Next, we analyse the energy in the remaining region Ω_0. Again, we divide this region in two parts,

$$\begin{aligned}\Omega_0^- &:= \{(x_1,x_2)\in\Omega_0,\, x_1<0\},\\ \Omega_0^+ &:= \{(x_1,x_2)\in\Omega_0,\, x_1>\ell\}.\end{aligned}$$

We will show that the energy in both subregions goes to zero. For this purpose, it is enough to consider the part Ω_0^-; the same argument will hold in Ω_0^+. In subdomain Ω_0^-, let us compute the function $\varphi_\varepsilon(x) = v(dist(x,K)/\varepsilon)$ in polar coordinates, *i.e.* with $r = \|x\|$,

$$\varphi_\varepsilon(x) = v(r/\varepsilon),$$

$$\Delta\varphi_\varepsilon(x) = \left(\frac{\partial^2}{\partial r} + \frac{1}{r}\frac{\partial}{\partial r}\right)\Big(v(r/\varepsilon)\Big) = \frac{1}{\varepsilon^2}v''(r/\varepsilon) + \frac{1}{\varepsilon r}v'(r/\varepsilon).$$

Next, we estimate in polar coordinates, still denoting by $T := diam(\Omega)$,

$$\begin{aligned}\int_{\Omega_0^-}(\varepsilon^3|\Delta\varphi_\varepsilon|^2+\frac{(1-\varphi_\varepsilon)^2}{\varepsilon})\,dx &\le \int_0^T\left(\int_{\frac{\pi}{2}}^{\frac{3\pi}{2}}\left(\varepsilon^3|\Delta\varphi_\varepsilon|^2+\frac{(1-\varphi_\varepsilon)^2}{\varepsilon}\right)rd\theta\right)dr\\ &= \pi\int_0^T\left(\varepsilon^3\left|\frac{1}{\varepsilon^2}v''(r/\varepsilon)+\frac{1}{\varepsilon r}v'(r/\varepsilon)\right|^2+\frac{(1-v(r/\varepsilon))^2}{\varepsilon}\right)rdr\\ &= \pi\varepsilon\int_0^{T/\varepsilon}\left(z\left|v''(t)+\frac{1}{t}v'(t)\right|^2+(1-v(t))^2t\right)dt.\end{aligned}$$

To analyse the limit in ε of the above upper bound, we recall the exact expression of v:

$$v(t)=1-\sqrt{2}e^{-\frac{t}{\sqrt{2}}}\sin\left(\frac{t}{\sqrt{2}}+\frac{\pi}{4}\right).$$

In particular,

$$(1-v(t))^2t\le Cte^{-\sqrt{2}t}.$$

Since the right-hand side of the previous inequality is in $L^1(0,+\infty)$, this upper bound implies that

$$\lim_{\varepsilon\to0}\pi\varepsilon\int_0^{T/\varepsilon}(1-v(t))^2tdt=0.$$

In a similar way, we can prove that the function $t\in(0,+\infty)\mapsto t|v''(t)|^2$ is integrable, so that

$$\lim_{\varepsilon\to0}\pi\varepsilon\int_0^{T/\varepsilon}t(v''(t))^2dt=0.$$

Finally,

$$v'(t)=e^{-\frac{t}{\sqrt{2}}}\left(\sin\left(\frac{t}{\sqrt{2}}+\frac{\pi}{4}\right)-\cos\left(\frac{t}{\sqrt{2}}+\frac{\pi}{4}\right)\right),$$

so that using the power series expansions of the functions sin and cos at point $t=\pi/4$, we obtain that the mapping $t\mapsto\frac{1}{t}v'(t)$ admits a limit when t goes to 0. Besides, $\frac{1}{\sqrt{t}}(v'(t))^2=O(\frac{1}{t^2})$ as $t\to+\infty$. This is enough to conclude that

$$\lim_{\varepsilon\to0}\pi\varepsilon\int_0^{T/\varepsilon}t\left|\frac{1}{t}v'(t)\right|^2dt=0.$$

Gathering the estimates in Ω_1, Ω_0^+ and Ω_0^+, we obtain the desired result:

$$\limsup_{\varepsilon\to0}\int_\Omega(\varepsilon^3|\Delta\varphi_\varepsilon|^2+\frac{(1-\varphi_\varepsilon)^2}{\varepsilon})\,dx\le2\ell m_{2D}.$$

□

2.3 Analysis of the second-order functional in dimension 3

In this section, we discuss the extension of the previous result in dimension 3. To this aim, we address the Γ-convergence of the second-order functional in dimension 3, which is now defined by

$$G_\varepsilon(u):=\int_\Omega\varepsilon^2|\Delta u|^2+\frac{(1-u)^2}{\varepsilon^2}\,dx+\frac{1}{\lambda_\varepsilon}\int_K(u^2+\delta_\varepsilon)d\mathcal{H}^1.$$

We are able to prove the Γ-convergence of this functional, under the hypothesis that the one-dimensional optimal profile satisfies a certain estimate (see (2.26)), that will be discussed in Section 2.3.2.

2.3.1 Existence of a one-dimensional optimal profile

Assume that K is a line in $\mathbb{R}^3$; for instance, $K = \mathbb{R}e_1$. Then, a function u of the form (2.8) is constant in the e_1 direction, and introducing the cylindrical coordinates (x_1, r, θ) of a point $x = (x_1, x_2, x_3)$, defined by $(x_2, x_3) = (r\cos\theta, r\sin\theta)$, the function u satisfies $u(x) = v(r)$. To compute the energy of such function u in $\mathbf{e}_1^\perp$, we compute the Laplace operator in polar coordinates:

$$\Delta u(x) = v''(r) + \frac{1}{r}v'(r).$$

Therefore, the energy in $\mathbf{e}_1^\perp$ is

$$\frac{1}{\varepsilon^\gamma}v^2(0) + \delta_\varepsilon + 2\pi\int_0^{+\infty}\left[\varepsilon^2\big(v''(r) + \frac{1}{r}v'(r)\big)^2 + \frac{1}{\varepsilon^2}(1-v(r))^2\right] r\,dr. \tag{2.18}$$

This motivates the definition of the following variational problem:

$$m_{3D} := \left\{\begin{array}{l} \min\limits_v E_{3D} := \displaystyle\int_0^{+\infty}\big[\big(v''(r) + \frac{1}{r}v'(r)\big)^2 + \big(1-v(r)\big)^2\big]\, r\,dr\,, \\ v \in H^2_{loc}((0,+\infty))\ ,\ v(0) = 0\ ,\ v'(0) = 0\ ,\ \lim\limits_{r\to+\infty} v(r) = 1. \end{array}\right. \tag{2.19}$$

The above problem m_{3D} cannot be solved explicitely as easily as the corresponding two-dimensional problem m_{2D}. However, it is possible to prove the existence of a minimizer.

Lemma 2.10. *There exists a unique solution $v \in H^2_{loc}(0,+\infty)$ to problem (2.19). In particular, m_{3D} is finite and positive.*

Proof. In order to simplify the expression of the energy, we first consider $\psi := v - 1$ and then use the change of variable

$$r = e^t \quad \text{and} \quad w(t) := \psi(e^t).$$

We deduce that

$$\begin{aligned}\int_0^{+\infty}\big[\big(v''(r) + \frac{1}{r}v'(r)\big)^2 + \big(v(r)-1\big)^2\big]\, r\,dr &= \int_{-\infty}^{+\infty}\big[\big(\psi''(e^t) + e^{-t}\psi'(e^t)\big)^2 + \big(\psi(e^t)\big)^2\big]\, e^{2t}\,dt \\ &= \int_{-\infty}^{+\infty}\big[e^{-2t}w''(t)^2 + e^{2t}w(t)^2\big]\,dt \end{aligned}\tag{2.20}$$

where we have used that

$$w'(t) = e^t\varphi'(e^t) \quad \text{and} \quad w''(t) = e^t\varphi'(e^t) + e^{2t}\varphi''(e^t).$$

Therefore, the minimization problem which defines m_{3D} is equivalent to the following one

$$m_{3D} := \left\{\begin{array}{c} \min\limits_w Q(w) := \displaystyle\int_{\mathbb{R}}\big[e^{-2t}w''(t)^2 + e^{2t}w(t)^2\big]\,dt, \\ w \in H^2_{loc}(\mathbb{R})\ ,\ \lim\limits_{t\to-\infty} w(t) = -1\ ,\ \lim\limits_{t\to-\infty} e^{-t}w'(t) = 0\ ,\ \lim\limits_{t\to+\infty} w(t) = 0. \end{array}\right.$$

We first notice that the infimum is not $-\infty$ because Q is nonnegative, and it is not $+\infty$ because there exist admissible w such that $Q(w) < +\infty$ (for instance, any function w such that $w(t) = -1$ for $t < 0$,

$w(t) = 0$ for $t > 0$ and w realises a smooth transition between -1 and 0 for $t \in [0, 1]$). Now let $(w_n)_{n\in\mathcal{N}}$ be a minimizing sequence. We can assume that for any $n \in \mathcal{N}$, w_n is of class C^2 on $\mathbb{R}$ and that there exists a constant $C > 0$ such that $Q(w_n) < C$ for all n. This means in particular that, for all $T > 0$,

$$\int_{-T}^{T} \left[e^{-2t} w_n''(t)^2 + e^{2t} w_n(t)^2\right] dt \leq C \tag{2.21}$$

therefore

$$\|w_n\|_{L^2(-T,T)} + \|w_n''\|_{L^2(-T,T)} \leq C(T),$$

for some constant $C(T)$ depending only on T. By Gagliardo-Nirenberg inequality, this implies that for every $T > 0$, w_n is bounded in $H^2(-T, T)$. Furthermore, by the compact embedding of $H^2(-T, T)$ into $C^{1,\alpha}([-T, T])$ for $\alpha < 1/2$, we can extract a (not relabeled) subsequence such that w_n converges strongly in $C^{1,\alpha}([-T, T])$ to some function w. Replacing T by a sequence $T_n \to +\infty$ and then extracting a diagonal subsequence, we can extract a further subsequence w_n, which converges now strongly to w in $C^{1,\alpha}([-T, T])$ for all $T > 0$. We also know that w_n'' converges weakly in $L^2(-T, T)$, for all T, to some limit $\zeta \in L^2_{loc}(\mathbb{R})$. This limit is equal to w'' in the sense of distributions, thus $w \in H^2_{loc}(\mathbb{R})$ and w_n'' converges weakly in $L^2(-T, T)$ to w'', for all T. Passing to the liminf in n for T fixed, we infer that

$$\int_{-T}^{T} \left[e^{-2t} w''(t)^2 + e^{2t} w(t)^2\right] dt \leq \liminf_{n\to+\infty} \int_{-T}^{T} \left[e^{-2t} w_n''(t)^2 + e^{2t} w_n(t)^2\right] dt. \tag{2.22}$$

But now, for all $\varepsilon > 0$ fixed, there exists $N \in \mathcal{N}$ such that $Q(w_n) \leq \inf Q + \varepsilon$ for all $n \geq N$. Passing to the $\liminf$ in n and using (2.22), we obtain

$$\int_{-T}^{T} \left[e^{-2t} \big(w'(t)\big)^2 + w(t)^2 e^{2t}\right] dt \leq \liminf_{n\to+\infty} G(w_n) \leq \inf Q + \varepsilon.$$

Letting $T \to +\infty$ and $\varepsilon \to 0$, we conclude that $Q(w) = \inf Q$.

To prove that w is a minimizer, it remains to check that w satisfies the conditions at $\pm\infty$. To treat the condition at $+\infty$, we go back to the function u, independent on x_1 and satisfying $u(x_1, x_2, x_3) = v(\sqrt{x_2^2 + x_3^2})$. Using computations (2.20) and formula (2.18), we see that

$$2\pi\, Q(w) = \int_{\mathbb{R}^2} \left[|\Delta u|^2 + (1 - u)^2\right] dx_2\, dx_3.$$

Noticing that $\|\Delta u\|_{L^2(\mathbb{R}^2)} = \|D^2 u\|_{L^2(\mathbb{R}^2)}$ and applying Gagliardo-Nirenberg inequality to the function $1-u$, we obtain that $1-u \in H^2(\mathbb{R}^2)$. By Sobolev imbedding theorem, this implies that for all $q \in (2, +\infty)$, $1 - u \in W^{1,q}(\mathbb{R}^2)$). Then, using the continuous imbedding of $W^{1,q}(\mathbb{R}^2)$ in $L^\infty(\mathbb{R}^2)$ and the density of $C_c(\mathbb{R}^2)$ in $W^{1,q}(\mathbb{R}^2)$, we get

$$\lim_{R\to+\infty} \|1 - u\|_{L^\infty(\mathbb{R}^2\setminus B_R(0))} = 0,$$

where $B_R(0)$ stands for the closed ball of center 0 and radius R in $\mathbb{R}^2$. Since u is radial, by definition of w, this implies that $\lim_{t\to+\infty} w(t) = 0$.

To treat the conditions at $-\infty$, we need to use the conditions satisfied by each function w_n, and get some uniform estimates ensuring the preservation of these conditions for the limit w. For that purpose, we first notice that from condition $\lim_{t\to-\infty} e^{-t}\, w_n(t)$, it is clear that

$$\lim_{t\to-\infty} w_n'(t) = 0.$$

Next, we use the bound

$$\sup_{n\in\mathcal{N}} \int_{-\infty}^{0} e^{-2t} w_n''(t)^2 dt \leq C, \tag{2.23}$$

from which we get, for all $s < t \leq 0$

$$\begin{aligned} |w_n'(t) - w_n'(s)| &= \Big| \int_s^t w_n''(\tau) d\tau \Big| \\ &\leq \left(\int_s^t e^{2\tau} d\tau \right)^{\frac{1}{2}} \left(\int_s^t e^{-2\tau} w_n''(\tau)^2 d\tau \right)^{\frac{1}{2}} \leq Ce^t. \end{aligned}$$

Passing to the limit in $s \to -\infty$, we deduce that

$$|w_n'(t)| \leq Ce^t \qquad \text{for all } n \text{ and for all } t \leq 0. \tag{2.24}$$

But this implies, using now that $w_n(t) \to -1$ at $-\infty$,

$$|w_n(t) + 1| \leq C \int_{-\infty}^{t} e^{\tau} d\tau \leq Ce^t \qquad \text{for all } n \text{ and for all } t \leq 0.$$

Using the pointwise convergence of w_n to w and of w_n' to w', we can pass to the limit in n in the above inequalities, to obtain

$$|w'(t)| \leq Ce^t \qquad \text{for } t \leq 0 \tag{2.25}$$

and

$$|w(t) + 1| \leq C \int_{-\infty}^{t} e^{\tau} d\tau \leq Ce^t \qquad \text{for } t \leq 0,$$

which implies that $\lim_{t\to-\infty} w(t) = -1$, as desired.

Finally, let us check that $\lim_{t\to-\infty} e^{-t} w'(t) = 0$. For that purpose, we first use (2.25) to deduce that

$$\lim_{t\to-\infty} w'(t) = 0.$$

Next, we use a similar argument as before, directly on w instead of w_n, and write

$$\begin{aligned} |w'(t) - w'(s)| &= \Big| \int_s^t w''(\tau) d\tau \Big| \\ &\leq \left(\int_s^t e^{2\tau} d\tau \right)^{\frac{1}{2}} \left(\int_s^t e^{-2\tau} w''(\tau)^2 d\tau \right)^{\frac{1}{2}} \leq C(t)e^t, \end{aligned}$$

where

$$C(t) := \left(\int_{-\infty}^{t} e^{-2\tau} w''(\tau)^2 d\tau \right)^{\frac{1}{2}}.$$

Letting $s \to -\infty$ and then $t \to -\infty$, we finally get $\lim_{t\to-\infty} e^{-t} w'(t) = 0$.

Finally, the minimizer is unique because the functional Q is strongly convex in the w variable. □

2.3.2 Explicit optimal profile v and decreasing property

The expression of the optimal profile v defined as a minimizer of the energy

$$E_{3D} = \int_0^{+\infty} r\left[\left(v''(r) + \frac{1}{r}v'(r)\right)^2 + \left(1 - v(r)\right)^2\right] dr,$$

under the constraints $v(0) = v'(0) = 0$ and $\lim_{r\to+\infty} v(r) = 1$, can be derived explicitly. Indeed, the associated Euler equation reads

$$r^4 v^{(4)} + 2r^3 v^{(3)} - r^2 v'' + rv' + r^4 v = r^4,$$

which solutions (see [1], page 379, equation 9.9.4) are on the form

$$v(r) = 1 + c_1 ber(r) + c_2 bei(r) + c_3 ker(r) + c_4 kei(r).$$

Here, *ber*, *bei*, *ker* and *kei* are the Kelvin functions and the constants c_1,c_2,c_3,c_4 should be determined to ensure the previous boundary conditions. More precisely, *ber* and *bei* are respectively the real and the imaginary part of $J(re^{\frac{2i\pi}{4}})$ where J is the zero order Bessel function of the first kind. Similarly, *ker* and *kei* are the real and the imaginary parts of $K(re^{\frac{i\pi}{4}})$, where K is the zero order modified Bessel function of the second kind.

Finally, as the asymptotic expansion of *kei* around $r = 0$ is known to be of the form

$$kei(r) = -\frac{\pi}{4} + \frac{1}{4}(1 - \gamma + log(2) - log(r))r^2 + O(r^4),$$

where $\gamma \simeq 0.577$ is the Euler-Mascheroni constant, we deduce that the optimal profile v is given by

$$v(r) = 1 + \frac{4}{\pi} kei(r).$$

We can observe on the left picture of Figure 1 a comparison between the two optimal profiles obtained in dimension 2 and 3.

Moreover, recall that the asymptotic expansions of *kei* for large arguments satisfies (see 9.10.4, [1])

$$kei(r) = -\frac{\pi}{2r} e^{-\frac{r}{\sqrt{2}}} \left[f_2(r)\sin(\beta(r)) + g_2(r)\cos(\beta(r))\right],$$

where $\beta(r) = \frac{r}{\sqrt{2}} + \frac{\pi}{8}$, and where

$$\begin{cases} f_2(r) & \simeq 1 + \sum_{k\geq 1}(-1)^k \frac{\cos(k\pi/4)}{k!(8r)^k} \Pi_{\ell=1}^k (2\ell-1)^2, \\ g_2(r) & \simeq \sum_{k\geq 1}(-1)^k \frac{\sin(k\pi/4)}{k!(8r)^k} \Pi_{\ell=1}^k (2\ell-1)^2, \end{cases}$$

We can then deduce that *kei* have a exponential decay. More generally, using the recurrence relations between the derivatives of the Kelvin functions (see 9.9.15, [1]), we can obtain similar asymptotic expansions for kei' and kei'' and also deduce the exponential decay of the derivative of *kei*, which is illustrated on the right picture of figure 1. In particular, all this arguments expect that the optimal profile v satisfies

$$\int_0^{+\infty} r^2 \left(\left| v''(r) + \frac{2}{r}v'(r) \right|^2 + (1 - v(r))^2 \right) dr < +\infty. \tag{2.26}$$

Notice that estimate (2.26) is the analogue in dimension 3 of the previous bound

$$\int_0^{+\infty} r\left(\left|v''(r)+\frac{2}{r}v'(r)\right|^2+(1-v(r))^2\right)dr<+\infty$$

that was used in dimension 2 to eliminate the contribution of the energy at the "endpoints" of the segment K in the limsup.

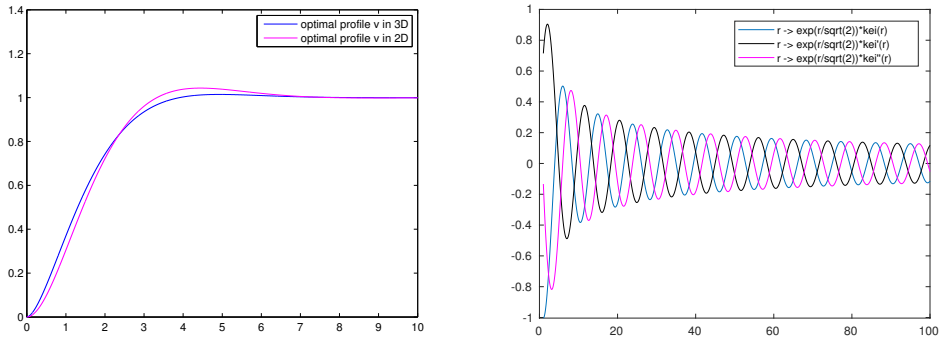

Figure 1: Left : comparison of the two optimal profiles obtained in dimension 2 and 3. Right: the function $r \mapsto e^{\frac{r}{\sqrt{2}}} kei(r)$

2.3.3 Discussion about the Γ-convergence in dimension 3

We expect that the methodology used in dimension 2 to prove the Γ-convergence can be extended in dimension 3 to get a similar result. More precisely, we expect that

$$\Gamma-\lim G_\varepsilon=\begin{cases}2\pi m_{3D}\mathcal{H}^1(K) & \text{if } u=1 \text{ a.e.},\\ +\infty & \text{otherwise,}\end{cases}$$

where m_{3D} is the constant defined in the minimizing problem (2.21) of the previous section. Indeed, the liminf inequality should follow by adapting the same argument and has no further difficulty.

We can then derive a limsup inequality in a similar way as we did in 2D. Let us write the details. As before we assume for simplicity that $K=[0,\ell]\times\{0\}$ and we divide Ω in two parts,

$$\Omega_1:=\Omega\cap\{(x_1,x_2,x_3)\in\Omega\ :\ x_1\in[0,1]\},$$
$$\Omega_0:=\Omega\setminus\Omega_1.$$

We set $T:=diam(\Omega)$ and compute the energy in Ω_1 and Ω_0 separately. We start with Ω_1; in this region, we use the cylindrical coordinates (x_1,r,θ) and define $\varphi_\varepsilon(x_1,x_2,x_3)=v(r/\varepsilon)$, where v is the minimizer

of problem (2.21). Then,

$$\begin{aligned}\int_{\Omega_1}(\varepsilon^2|\Delta\varphi_\varepsilon|^2+\frac{(1-\varphi_\varepsilon)^2}{\varepsilon^2})\,dx &\le \int_0^\ell\left(\int_0^T\int_0^{2\pi}\left(\varepsilon^2\left|\frac{1}{\varepsilon^2}v''\left(\frac{r}{\varepsilon}\right)+\frac{1}{\varepsilon r}v'(\frac{r}{\varepsilon})\right|^2+\frac{(1-v)^2}{\varepsilon^2}\right)\,rd\theta dr\right)dx_1\\ &= 2\pi\ell\int_0^T\varepsilon^2\left(\left|\frac{1}{\varepsilon^2}v''\left(\frac{r}{\varepsilon}\right)+\frac{1}{\varepsilon r}v'(\frac{r}{\varepsilon})\right|^2+\frac{(1-v)^2}{\varepsilon^2}\right)\,rdr\\ &= 2\pi\ell\int_0^{T/\varepsilon}\left(\left|v''(z)+\frac{1}{z}v'(z)\right|^2+(1-v(z))^2\right)zdz\\ &\longrightarrow_{\varepsilon\to0} 2\pi\ell m_{3D},\end{aligned}$$

which proves

$$\limsup_{\varepsilon\to0}\int_{\Omega_1}(\varepsilon^3|\Delta\varphi_\varepsilon|^2+\frac{(1-\varphi_\varepsilon)^2}{\varepsilon})\,dx\le 2\pi\ell m_{3D}.$$

It remains to analyze the energy in region Ω_0, exactly as for the 2D case. Once again, we divide this region in two parts:

$$\begin{aligned}\Omega_0^- &:= \{(x_1,x_2,x_3)\in\Omega_0,\,x_1<0\},\\ \Omega_0^+ &:= \{(x_1,x_2,x_3)\in\Omega_0,\,x_1>\ell\}.\end{aligned}$$

Let us show that the contributions of these subregions in the energy goes to zero as ε goes to zero. As the arguments are similar for both subregions, let us consider only Ω_0^-. In this domain, we compute the function $\varphi_\varepsilon(x)=v(dist(x,K)/\varepsilon)$ in spherical coordinates, *i.e.* (r,θ,α) with $r=\|x\|$. In these coordinates, the Laplace operator can be written as

$$\varphi_\varepsilon(x)=v(r/\varepsilon),$$

$$\Delta\varphi_\varepsilon(x)=\left(\frac{\partial^2}{\partial r}+\frac{2}{r}\frac{\partial}{\partial r}\right)\Big(v(r/\varepsilon)\Big)=\frac{1}{\varepsilon^2}v''(r/\varepsilon)+\frac{2}{\varepsilon r}v'(r/\varepsilon),$$

and the Jacobian determinant is $r^2|\sin(\alpha)|$. Hence,

$$\begin{aligned}\int_{\Omega_0^-}(\varepsilon^3|\Delta\varphi_\varepsilon|^2+\frac{(1-\varphi_\varepsilon)^2}{\varepsilon})\,dx &\le \pi\int_0^T\int_0^\pi\left(\varepsilon^3\left|\frac{1}{\varepsilon^2}v''(r/\varepsilon)+\frac{2}{\varepsilon r}v'(r/\varepsilon)\right|^2+\frac{(1-v(r/\varepsilon))^2}{\varepsilon}\right)r^2|\sin(\alpha)|d\alpha dr\\ &\le \pi^2\varepsilon\int_0^{T/\varepsilon}t^2\left(\left|v''(t)+\frac{2}{t}v'(t)\right|^2+(1-v(t))^2\right)dt,\end{aligned}$$

and we conclude that this upper bound goes to 0 as $\varepsilon\to0$ thanks to (2.26). By the same computations, the same result holds in Ω_0^+.

As a conclusion, summing up the contributions of Ω_1 and Ω_0, we have proved that

$$\limsup_{\varepsilon\to0}\int_{\Omega}(\varepsilon^3|\Delta\varphi_\varepsilon|^2+\frac{(1-\varphi_\varepsilon)^2}{\varepsilon})\,dx\le 2\pi\ell m_{3D},$$

which finishes the proof of the limsup inequality in the 3D case.

2.4 Analysis of the regularized geodesic term

In this section we analyze the impact of replacing the term $\int_\Gamma (u^2+\delta_\varepsilon) d\mathcal{H}^1$ in the functional by the following regularized one

$$\int_\Gamma (u^2+\delta_\varepsilon)\; d(\mathcal{H}^1 * \rho_r),$$

which will be used in the numerical experiments. Here, $\rho_r(x) = \frac{1}{r^d}\rho(x/r)$ where ρ is a standard convolution kernel supported in the ball of radius one centered at the origin and d is the space dimension. Our goal is to identify a dependence between r and ε so that the difference between the original functional and the regularized one converges to zero as $\varepsilon \to 0$, in a certain sense.

2.4.1 Case of the first order functional in dimension 2

To simplify the analysis, we will only consider the case of two points a_0, a_1; the general case can be handled following exactly the same idea. In this context we will denote by E_ε the original energy

$$E_\varepsilon(u,\boldsymbol{\gamma}) := \varepsilon \int_\Omega |\nabla u|^2\, dx + \frac{1}{4\varepsilon}\int_\Omega (u-1)^2\, dx + \frac{1}{\lambda_\varepsilon}\int_{\Gamma(\gamma)} (\delta_\varepsilon + u^2)\, d\mathcal{H}^1, \tag{2.27}$$

and by $E_{\varepsilon,r}$ the regularized one

$$E_{\varepsilon,r}(u,\boldsymbol{\gamma}) := \varepsilon \int_\Omega |\nabla u|^2\, dx + \frac{1}{4\varepsilon}\int_\Omega (u-1)^2\, dx + \frac{1}{\lambda_\varepsilon}\int_{\Gamma(\gamma)} (\delta_\varepsilon + u^2)\, d(\mathcal{H}^1 * \rho_r). \tag{2.28}$$

In this section, we assume that $\boldsymbol{\gamma}$ is fixed and Ahlfors-regular with constant $\Lambda_\varepsilon = 4/\delta_\varepsilon$, as it is the case for a minimizer (Theorem 2.2). Notice also that for a sequence $(u_\varepsilon, \boldsymbol{\gamma}_\varepsilon)$ with bounded energy $E_\varepsilon(u_\varepsilon, \boldsymbol{\gamma}_\varepsilon) \le C$, the total length of $\Gamma(\boldsymbol{\gamma}_\varepsilon)$ is bounded by

$$\mathcal{H}^1(\Gamma(\boldsymbol{\gamma}_\varepsilon)) \le C\frac{\lambda_\varepsilon}{\delta_\varepsilon}.$$

To simplify the notation, we will write $E_\varepsilon(u)$ instead of $E_\varepsilon(u,\boldsymbol{\gamma})$ and Γ instead of $\Gamma(\gamma)$. We want to study the difference between a minimizer of E_ε and a minimizer of $E_{\varepsilon,r}$, in the u variable. More precisely, our goal is to prove the following.

Proposition 2.11. *Let Γ be the support of an Ahlfors-regular curve with constant $4/\delta_\varepsilon$ and length bounded by $\mathcal{H}^1(\Gamma) \le C\frac{\lambda_\varepsilon}{\delta_\varepsilon}$. Then for any $r>0$, the functional $E_{\varepsilon,r}$ admits a minimizer $u_{\varepsilon,r} \in 1 + H^1_0(\Omega)$, and*

$$E_\varepsilon(u_{\varepsilon,r}) \le \min E_\varepsilon + C\frac{r^\alpha}{\delta_\varepsilon^2 \varepsilon^\alpha}$$

for all $\alpha \in (0,1)$ (with C depending on α). In particular, if $r_\varepsilon \to 0$ in such a way that $r_\varepsilon = o(\varepsilon \delta_\varepsilon^{\frac{2}{\alpha}})$, then

$$E_\varepsilon(u_{\varepsilon,r_\varepsilon}) - \min E_\varepsilon \to 0.$$

Proof. Let us only give the ideas of the proof relying on the techniques deployed in [4], since the full details would require a too long exposition. To prove the existence of a minimizer $u_{\varepsilon,r}$ for $E_{\varepsilon,r}$, one can follow the argument already used in [4] for E_ε, that we recall briefly. The first step is to prove that

$\mathcal{H}^1|_\Gamma \in W^{-1,p}(\Omega)$ for all $p \geq 1$; then, by use of elliptic estimates, one can deduce the existence of a minimizer $\bar{u}_\varepsilon \in 1 + H^1_0(\Omega)$ for E_ε, which also belongs to $C^{0,\alpha}$ for all $\alpha \in (0,1)$ with the estimate

$$\|u_\varepsilon\|_{C^{0,\alpha}} \leq C_\alpha \frac{1}{\lambda_\varepsilon \delta_\varepsilon \varepsilon^\alpha}. \tag{2.29}$$

We refer to [4, Proposition 2.10] for more details.

Now, concerning the modified functional $E_{\varepsilon,r}$, we start by observing that for any $p \geq 1$,

$$\|\mathcal{H}^1|_\Gamma * \rho_r\|_{W^{-1,p}} \leq \|\mathcal{H}^1|_\Gamma\|_{W^{-1,p}}, \quad \forall r > 0. \tag{2.30}$$

Indeed, it is well known that for any $\varphi \in W^{1,p}_0(\Omega)$ and $r > 0$, there holds

$$\|\varphi * \rho_r\|_{W^{1,p}} \leq \|\varphi\|_{W^{1,p}},$$

from which we deduce the estimate

$$|\langle \mathcal{H}^1|_\Gamma * \rho_r, \varphi\rangle| \quad = \quad |\langle \mathcal{H}^1|_\Gamma, \varphi * \rho_r\rangle| \leq \|\mathcal{H}^1|_\Gamma\|_{W^{-1,p}} \|\varphi\|_{W^{1,p}}. \tag{2.31}$$

This proves (2.30) by duality.

A consequence of (2.30) is that, reproducing the proof of [4, Proposition 2.10] one can establish the existence of a minimizer $u_{\varepsilon,r} \in (1 + H^1_0(\Omega)) \cap L^\infty(\Omega)$ satisfying the same estimate as u_ε, namely

$$\|u_{\varepsilon,r}\|_{C^{0,\alpha}} \leq C_\alpha \frac{1}{\lambda_\varepsilon \delta_\varepsilon \varepsilon^\alpha}. \tag{2.32}$$

On the other hand, for any $v \in C^{0,\alpha}(\mathbb{R}^2)$ and $x \in \mathbb{R}^2$, there holds

$$|v * \rho_r(x) - v(x)| \leq \int_{\mathbb{R}^2} |v(x-y) - v(x)| \rho_r(y) dy = \int_{B_r(0)} |v(x-y) - v(x)| \rho_r(y) dy \leq \|v\|_{C^{0,\alpha}} r^\alpha.$$

Therefore, for any $v \in C^{0,\alpha}(\mathbb{R}^2)$,

$$\Big| \int_\Gamma v \, d\mathcal{H}^1 - \int_\Gamma v \, d(\mathcal{H}^1 * \rho_r) \Big| \leq \int_\Gamma |v - v * \rho_r| d\mathcal{H}^1 \leq \|v\|_{C^{0,\alpha}} r^\alpha \mathcal{H}^1(\Gamma). \tag{2.33}$$

Noticing that $\|u^2_{\varepsilon,r}\|_{C^{0,\alpha}} \leq C\|u_{\varepsilon,r}\|_{C^{0,\alpha}}$, $\|u^2_\varepsilon\|_{C^{0,\alpha}} \leq C\|u_\varepsilon\|_{C^{0,\alpha}}$, and applying the above estimate to $u^2_{\varepsilon,r}$ and then to u^2_ε, we obtain

$$\begin{aligned}
E_\varepsilon(u_{\varepsilon,r}) &\leq E_{\varepsilon,r}(u_{\varepsilon,r}) + \int_\Gamma u^2_{\varepsilon,r} \, d\mathcal{H}^1 - \int_\Gamma u^2_{\varepsilon,r} \, d(\mathcal{H}^1 * \rho_r) \\
&\leq E_{\varepsilon,r}(u_{\varepsilon,r}) + C\|u_{\varepsilon,r}\|_{C^{0,\alpha}} r^\alpha \mathcal{H}^1(\Gamma) \qquad \text{thanks to (2.33)}, \\
&\leq E_{\varepsilon,r}(u_\varepsilon) + C\|u_{\varepsilon,r}\|_{C^{0,\alpha}} r^\alpha \mathcal{H}^1(\Gamma) \qquad \text{because } \bar{u}_{\varepsilon,r} \text{ is a minimizer}, \\
&\leq E_\varepsilon(u) + C(\|u_{\varepsilon,r}\|_{C^{0,\alpha}} + \|u_\varepsilon\|_{C^{0,\alpha}}) r^\alpha \mathcal{H}^1(\Gamma), \qquad \text{by (2.33) again},
\end{aligned}$$

and this together with (2.29) and (2.32) concludes the proof of the proposition. □

2.4.2 Remark on the second order Cahn Hillard functional in dimension 2

In the context of the second order functional in dimension 2, the original energy G_ε reads as

$$G_\varepsilon(u,\boldsymbol{\gamma}) := \varepsilon^3 \int_\Omega |\Delta u|^2\, dx + \frac{1}{4\varepsilon}\int_\Omega (u-1)^2\, dx + \frac{1}{\lambda_\varepsilon}\int_{\Gamma(\gamma)} (\delta_\varepsilon + u^2)\, d\mathcal{H}^1,$$

and its regularized versus $G_{\varepsilon,r}$ is given by

$$G_{\varepsilon,r}(u,\boldsymbol{\gamma}) := \varepsilon^3 \int_\Omega |\Delta u|^2\, dx + \frac{1}{4\varepsilon}\int_\Omega (u-1)^2\, dx + \frac{1}{\lambda_\varepsilon}\int_{\Gamma(\gamma)} (\delta_\varepsilon + u^2)\, d(\mathcal{H}^1 * \rho_r).$$

Our interest of these 2 new models is to improve the regularity of its solution u_ε which are expected now at least C^1 (if γ is sufficiently smooth) and with a bound inequality of the form

$$\|u_\varepsilon\|_{C^1} \leq \frac{C}{\varepsilon}.$$

In particular, this same reasoning as previously gives now an estimation of the form

$$G_\varepsilon(u_{\varepsilon,r}) \leq G_\varepsilon(u) + C(\|u_{\varepsilon,r}\|_{C^1} + \|u_\varepsilon\|_{C^1}) r\ \mathcal{H}^1(\Gamma),$$

and conduces to

$$G_\varepsilon(u_{\varepsilon,r}) \leq \min G_\varepsilon + C\frac{r}{\varepsilon},$$

when $\mathcal{H}^1(\Gamma(\boldsymbol{\gamma}_\varepsilon)) \leq C$, which is a reasonable assumption.

In particular, if $r_\varepsilon \to 0$ in such a way that $r_\varepsilon = o(\varepsilon)$, then

$$G_\varepsilon(u_{\varepsilon,r_\varepsilon}) - \min G_\varepsilon \to 0.$$

3 Numerical experiments

The motivation of this section is to explain how to compute the solution of the PDE

$$\begin{cases} u_t = -\nabla_u \overline{E}_\varepsilon(u,\boldsymbol{\gamma}) \\ \boldsymbol{\gamma} = \mathrm{Argmin}_{\boldsymbol{\gamma}}\{E_\varepsilon(u,\boldsymbol{\gamma})\}. \end{cases}$$

where $\overline{E}_\varepsilon(u,\boldsymbol{\gamma})$ is equal to

- Case 1 : Cahn-Hilliard of order 1 and classical smooth geodesic term

$$\overline{E}_\varepsilon(u,\boldsymbol{\gamma}) = P_\varepsilon(u) + \tilde{R}_\varepsilon(u,\boldsymbol{\gamma}),$$

- Case 2 : Cahn-Hilliard of order 2 and classical smooth geodesic term

$$\overline{E}_\varepsilon(u,\boldsymbol{\gamma}) = \tilde{P}_\varepsilon(u) + \tilde{R}_\varepsilon(u,\boldsymbol{\gamma}),$$

- Case 3 : Cahn-Hilliard of order 2 and concentrated smooth geodesic term

$$\overline{E}_\varepsilon(u,\boldsymbol{\gamma}) = \tilde{P}_\varepsilon(u) + \tilde{R}_{\varepsilon,\max}(u,\boldsymbol{\gamma}).$$

In each situation, we consider the solution at all time $t \in [0,T]$ in a computation bow Q with periodic boundary conditions, associated with the initial condition $u(x,0) = 1$. We now focus on the first cases but the other one are very similar.

As explained previously, our numerical approach is based on a splitting method, which constructs the approximative sequence $(u^n, \boldsymbol{\gamma}^n)$ of $(u, \boldsymbol{\gamma})$ at time $n\delta_t$ recursively, as follows:

Step 1 : Computation of $\boldsymbol{\gamma}^n$ as

$$\boldsymbol{\gamma}^n = \min_{\boldsymbol{\gamma} \in \mathcal{P}(a_0,\mu)} \{E_\varepsilon(u^n, \boldsymbol{\gamma})\}.$$

Step 2 : Computation of function u^{n+1} defined by $u^{n+1} = v(\delta_t)$ where v is solution of the following PDE:

$$\begin{cases} v_t = 2\varepsilon\Delta v - \frac{1}{2\varepsilon}(v-1) - \frac{2}{\lambda_\varepsilon}\omega^\varepsilon[\boldsymbol{\gamma}^n]v \\ v(.,0) = u^n(.) \end{cases}$$

Recall that $\omega^\varepsilon[\boldsymbol{\gamma}^n]$ is defined by (1.12).

3.1 Numerical scheme

In this section, we give more details on the computation of the geodesic $\boldsymbol{\gamma}^n$ and how to obtain an approximation of $u^{n+1} = v(\delta_t)$.

Computation of $\boldsymbol{\gamma}^n$
Recall that, in cases 1 and 2, the geodesics $\boldsymbol{\gamma}^n = \gamma_i^n$ are defined by

$$\boldsymbol{\gamma}^n = \min_{\boldsymbol{\gamma} \in \mathcal{P}(a_0,\mu)} \{E_\varepsilon(u^n, \boldsymbol{\gamma})\} = \min_{\boldsymbol{\gamma} \in \mathcal{P}(a_0,\mu)} \left\{\tilde{R}_\varepsilon(u^n, \boldsymbol{\gamma})\right\},$$

where

$$\begin{aligned} \tilde{R}_\varepsilon(u, \boldsymbol{\gamma}) &= \frac{1}{\lambda_\varepsilon}\int_\Omega \left[\sum_{i=1}^N (\rho_{\varepsilon^\alpha} * \mathcal{H}^1|_{\Gamma(\gamma_i)})\right](\delta_\varepsilon + u^2)\,dx \\ &= \frac{1}{\lambda_\varepsilon}\sum_{i=1}^N \int_{\Gamma(\gamma_i)} (\delta_\varepsilon + u^2) * \rho_{\varepsilon^\alpha}\, d\mathcal{H}^1. \end{aligned}$$

It shows that we can compute the geodesics γ_i^n in two steps.

We first compute the weighted distance function $x \to d_{x_0,\omega}(x)$ corresponding to the distance function from a point x_0 to x, associated to the weight $w = (\delta_\varepsilon + u^2) * \rho_{\varepsilon^\alpha}$. More precisely, this function can be defined as a viscosity solution of the following nonlinear Eikonal equation

$$|\nabla d_{x_0,\omega}(x)| = \omega(x), \text{ in } \Omega, \quad \text{with } d_{x_0,\omega}(x_0) = 0.$$

The approximation of $d_{x_0,\omega}$ is computed using a Fast Marching Method [14, 15, 2], which can be reformulated as a Dijkstra's algorithm. Notice that in practice, we use the *Toolbox Fast Marching* proposed by G. Peyre in the *Matlab* environment, available at
http://www.mathworks.com/matlabcentral/fileexchange/.

The second step consists in computing each geodesic $\gamma_i : [0,1] \to \Omega$ satisfying $\gamma^i(0) = x_0$, $\gamma^i(1) = x_i$, associated with the distance $d_{x_0,\omega}$. This can be achieved using that the derivative of $\gamma^i(s)$ is directed by $\nabla d_{x_0,\omega}(\gamma^i(s))$ for all $s \in [0,1]$. In practice, we use the *Matlab* function *compute_geodesic* from *Fast Marching Toolbox* to compute an approximation of each geodesic.

Remark 3.1. *The minimization of the geodesic term $\tilde{R}^{\mu}_{\varepsilon,max}(u,\boldsymbol{\gamma})$ with respect to $\boldsymbol{\gamma}$ is not as simple as the minimization of $\tilde{R}^{\mu}_{\varepsilon}(u,\boldsymbol{\gamma})$, since the optimal geodesics γ_i are now coupled. As a result, the optimal geodesics for $\tilde{R}^{\mu}_{\varepsilon,max}$ appear very complicated to compute in practice. Hence, even if the solutions are not optimal, we always update the geodesics by minimizing the uncoupled term $\tilde{R}^{\mu}_{\varepsilon}$.*

Computation of u^{n+1}

In order to get a high accuracy approximation in space, we use a semi-implicit Fourier-spectral method. For instance, we can define the approximation of u^{n+1} as follows :

$$\frac{u^{n+1}-u^n}{\delta_t} = 2\varepsilon\Delta u^{n+1} - \frac{1}{2\varepsilon}(u^{n+1}-1) - \alpha u^{n+1} - \left(\frac{2}{\lambda_\varepsilon}\omega^\varepsilon[\boldsymbol{\gamma}^n] - \alpha\right)u^n,$$

where α can be viewed as a stabilization parameter for the scheme. Indeed, it is well known [10, 16] that if the explicit part is the L^2-gradient flow of a concave functional, then the global numerical scheme appears to be stable without any condition on the time step δ_t. Here, stability is a stability in the sense of the associated energy, which is nonincreasing during iterations. In our situation, the explicit term is identified to

$$-\left(\frac{2}{\lambda_\varepsilon}\omega^\varepsilon[\boldsymbol{\gamma}^n] - \alpha\right)u^n,$$

and can be viewed as the L^2-gradient of

$$J_{\text{explicit}}(u) = \int_\Omega \left(\frac{1}{\lambda_\varepsilon}\omega^\varepsilon[\boldsymbol{\gamma}^n] - \frac{\alpha}{2}\right)u^2 dx,$$

which is clearly concave as soon as

$$\alpha \geq \sup_{x\in\Omega}\left\{\frac{2}{\lambda_\varepsilon}\omega^\varepsilon[\boldsymbol{\gamma}^n]\right\}.$$

Remark 3.2. *Such parameter α exists because by regularization, $\omega^\varepsilon[\boldsymbol{\gamma}^n]$ is a bounded function. This is the main reason why we chose to regularize the geodesic terms.*

Finally, the approximation u^{n+1} satisfies

$$u^{n+1} = \left(I_d + \delta_t\left(-2\varepsilon\Delta + \frac{1}{2\varepsilon} + \alpha\right)\right)^{-1}\left(u^n + \delta_t\left(\frac{1}{2\varepsilon} - \left(\frac{2}{\lambda_\varepsilon}\omega^\varepsilon[\boldsymbol{\gamma}^n] - \alpha\right)u^n\right)\right),$$

where the operator $\left(I_d + \delta_t\left(-2\varepsilon\Delta + \frac{1}{2\varepsilon} + \alpha\right)\right)^{-1}$ can be computed in Fourier space by using a multiplication with the symbol σ defined by

$$\sigma(\xi) = \frac{1}{1 + \delta_t\left(2\varepsilon(4\pi^2|\xi|^2) + \frac{1}{2\varepsilon} + \alpha\right)}.$$

Remark 3.3. *Cases 2 and 3 using the Ambrosio-Torterelli approximation $\tilde{P}_\varepsilon(u)$ conduce to a similar symbol $\tilde{\sigma}$ defined by*

$$\tilde{\sigma}(\xi) = \frac{1}{1 + \delta_t\left(2\varepsilon^{2p-1}((4\pi^2)|\xi|^2)^p + \frac{1}{2\varepsilon} + \alpha\right)}.$$

Spatial discretization and Fourier space

We recall that the P Fourier approximation of a $2D$ function u in a box $Q = [0, L_1] \times [0, L_2]$ is given by

$$u^P(x) = \sum_{p_1,p_2=-P/2+1}^{P/2} c_{\mathbf{p}} e^{2i\pi\xi_{\mathbf{p}}\cdot x}$$

where $\mathbf{p} = (p_1, p_2)$ and $\xi_{\mathbf{p}} = (p_1/L_1, p_2/L_2)$. Here $c_{\mathbf{p}}$ represents the P^2 first discrete Fourier coefficients of u. Moreover, the inverse discrete Fourier transform of $c_{\mathbf{p}}$ leads to $u^P_{\mathbf{p}} = IFFT[c_{\mathbf{p}}]$ where $u^P_{\mathbf{p}}$ is the value of u at the points $x_{\mathbf{p}} = (p_1 h_1, p_2 h_2)$ and $h_j = L_j/P$ for $j \in \{1, 2\}$. Conversely, $c_{\mathbf{p}}$ can be computed by applying the discrete Fourier transform to $u^P_{\mathbf{p}}$:

$$c_{\mathbf{p}} = FFT[u^P_{\mathbf{p}}].$$

For instance, the operator $\left(I_d + \delta_t\left(-2\varepsilon\Delta + \frac{1}{2\varepsilon} + \alpha\right)\right)^{-1}$ can be computed in Fourier space by using

$$\left(I_d + \delta_t\left(-2\varepsilon\Delta + \frac{1}{2\varepsilon} + \alpha\right)\right)^{-1} u^P(x) = \sum_{p_1,p_2=-P/2+1}^{P} \frac{c_{\mathbf{p}}}{1 + \delta_t\left(2\varepsilon 4\pi^2|\xi_{\mathbf{p}}|^2 + \frac{1}{2\varepsilon} + \alpha\right)} e^{2i\pi\xi_{\mathbf{p}}\cdot x},$$

which can be done in practice by

$$\left(I_d + \delta_t\left(-2\varepsilon\Delta + \frac{1}{2\varepsilon} + \alpha\right)\right)^{-1} u^P(x_{\mathbf{p}}) = IFFT\left[\frac{FFT[u^P_{\mathbf{p}}]}{1 + \delta_t\left(2\varepsilon 4\pi^2|\xi_{\mathbf{p}}|^2 + \frac{1}{2\varepsilon} + \alpha\right)}\right].$$

3.2 Geodesics and optimal profile

Fast marching method and computation of geodesics

In Figure 2, we give a first example of computation of a geodesic between two points $x_0 = [-0.7, 0.7]$ and $x_1 = [0.7, -0.7]$, associated to the weight function $w = \|x\|^2$. We apply the algorithm in a box $Q = [-1, 1]^2$, with a discretization step $h = 2/P$ for $P = 2^{10}$. We plot on the left picture the function w, and on the right, the distance function d_{ω,x_0} and the computed geodesic γ_1. As explained previously, we can clearly observe that γ_1 is orthogonal to the level sets of d_{ω,x_0}.

Optimal profile

We now consider the problem of computing the phase field function $u^\varepsilon_{\boldsymbol{\gamma}}$ associated to a given geodesic $\boldsymbol{\gamma}$ and defined as a minimizer of $\overline{E}_\varepsilon(u, \boldsymbol{\gamma})$. We only consider here the case of one geodesic $\boldsymbol{\gamma} = \gamma_1$, which restricts our analysis to the first and second cases. Moreover, the solution $u^\varepsilon_{\gamma_1}$ can be computed as the stationary limit of the function v, defined as the solution of the PDE

$$\begin{cases} v_t = 2\varepsilon\Delta v - \frac{1}{2\varepsilon}(v-1) - \frac{2}{\lambda_\varepsilon}\omega^\varepsilon[\boldsymbol{\gamma}^n]v \\ v(.,0) = 1, \end{cases}$$

in the first case and of

$$\begin{cases} v_t = -2\varepsilon^3\Delta v^2 - \frac{1}{2\varepsilon}(v-1) - \frac{2}{\lambda_\varepsilon}\omega^\varepsilon[\boldsymbol{\gamma}^n]v \\ v(.,0) = 1, \end{cases}$$

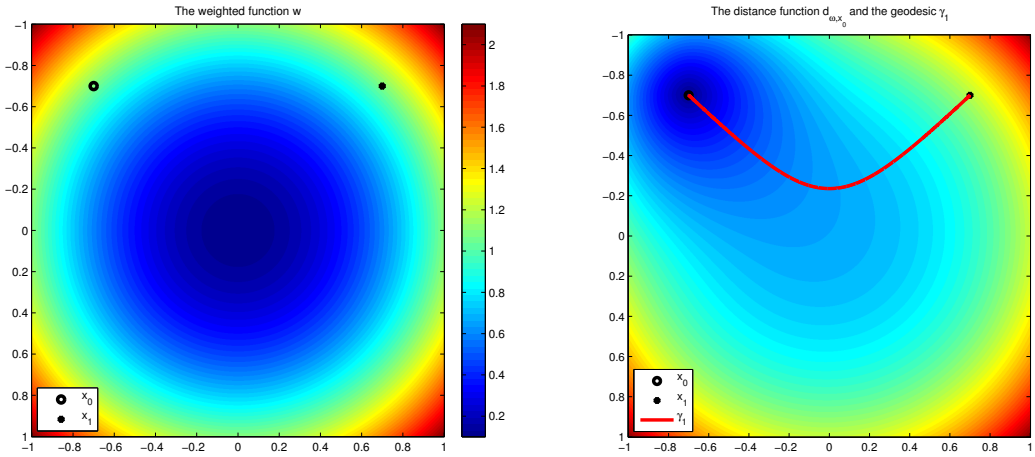

Figure 2: Numerical example of geodesic computation. Left: the weight function $w = \|x\|^2$ and the endpoints $x_0 = [-0.7, 0.7]$ and $x_1 = [0.7, -0.7]$. Right: the distance function d_{ω,x_0} computed using a fast Marching algorithm, and the geodesic γ_1 between x_0 and x_1.

in the second case.

In the first example, we consider ther case of dimension 1 with $Q = [-1, 1]$, $P = 2^{10}$, $\lambda_\varepsilon = \varepsilon^2$ and $\Gamma[\gamma_1] = \{0\}$. We plot in Figure 3 the function u^ε_γ obtained with the two models (in blue using $\varepsilon\Delta$ and in red using $\varepsilon^3\Delta^2$) and for different values of ε ($\varepsilon = 20/P$, $\varepsilon = 10/P$ and $\varepsilon = 5/P$). A first remark is that from a numerical point of view, the width of the diffuse interface depends linearly on ε. Moreover, the models give similar profiles; the main difference is that the profile obtained in case 2 is more regular, but its range is not contained in $[0, 1]$. We also present in Figure 4 some equivalent numerical experiments in dimension 2, and the conclusions are very similar.

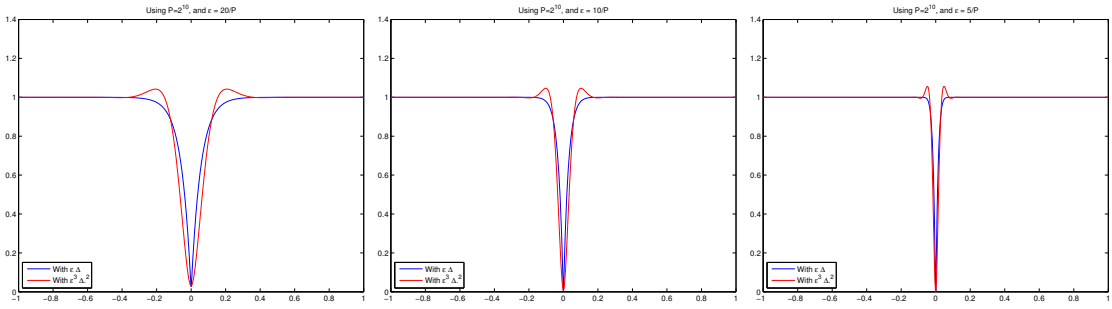

Figure 3: Comparison of optimal profiles $u^\varepsilon_{\{0\}}$ in dimension 1, for different values of ε and using the two different models. From left to right: $\varepsilon = 20/P$, $\varepsilon = 10/P$, $\varepsilon = 5/P$ with $P = 2^{10}$.

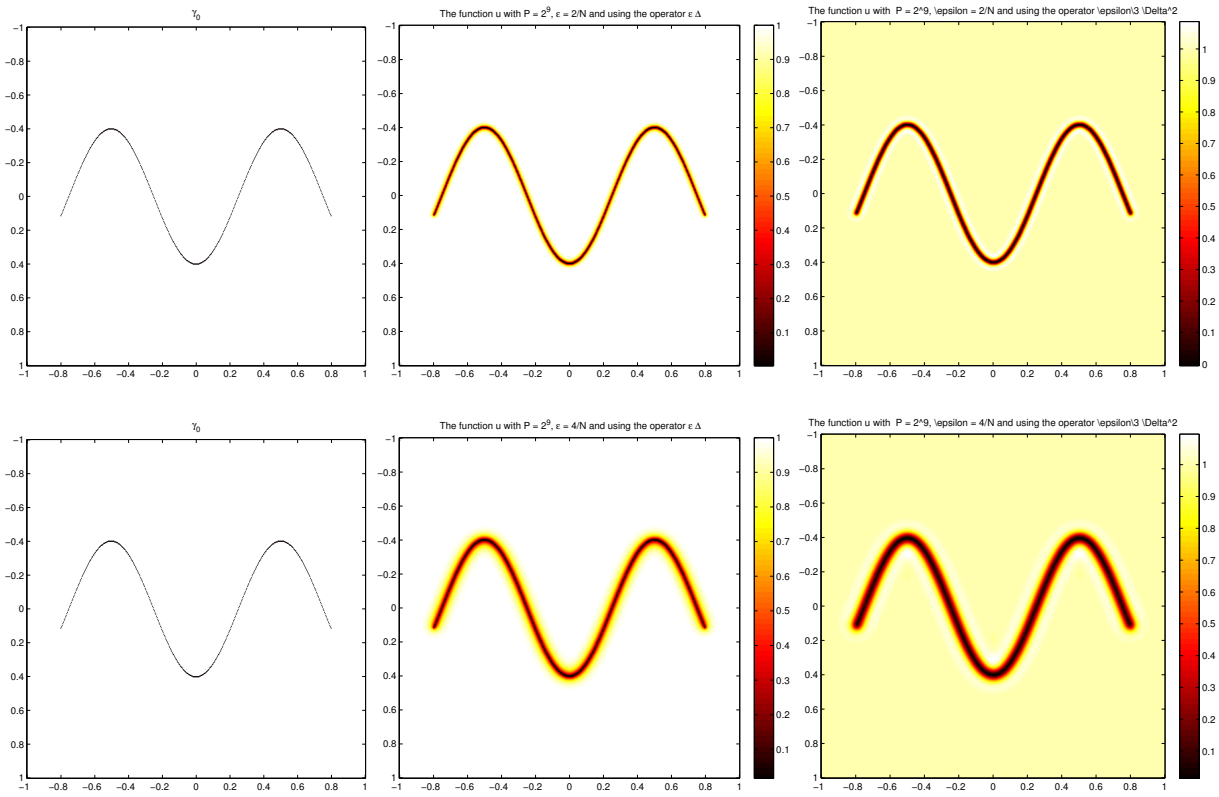

Figure 4: Comparison of optimal profiles $u^{\varepsilon}_{\{\gamma_1\}}$ in dimension 2, for different values of ε and using the two different models. Left: the geodesic γ_1; middle: $u^{\varepsilon}_{\{\gamma_1\}}$ obtained with the first model; right: $u^{\varepsilon}_{\{\gamma_1\}}$ obtained with the second model. First and second line with respectively $\varepsilon = 2/P$ and $\varepsilon = 4/P$, where $P = 2^9$.

3.3 First experiments and comparison of the two different Cahn-Hilliard functionals

The first numerical experiments concern simple configurations of 3,4 and 5 points. The results are plotted in Figure 5, 6 and 7. More precisely and in each case, we fix the set of parameters equal to $P = 2^7$, $\varepsilon = 6/P$, $\delta_t = \varepsilon$ and $\lambda_\varepsilon = \varepsilon^2$ at the beginning of the simulation, and we compute the solution u^n until convergence to a stationary solution u^ε. Then, we divide by 2 the value of ε and compute the new stationary solution associated to this value. Notice that in Figures 5, 6 and 7, the first and the second lines correspond respectively to the classical and to the second-order Edge-Penalization Cahn-Hilliard functional. The first three pictures of each line represent the phase field function u^n during the iterations associated to the first set of parameters. We also plot in the last picture the stationary solution associated to the second value of ε.

We observe that in each configuration, we numerically find the solution of the original Steiner problem,

which highlights the efficiency of the method. Moreover and as expected, the solution associated to the operator $-\varepsilon^3\Delta^2$ is smoother than the one obtained with the classical Cahn-Hilliard functional. This property should facilitate the discretization and it clearly accelerates the convergence of the method to the stationary solution. For that reasons, we will only consider the second-order Edge-Penalization Cahn-Hilliard functional $\tilde{P}_\varepsilon$ in the rest of the paper.

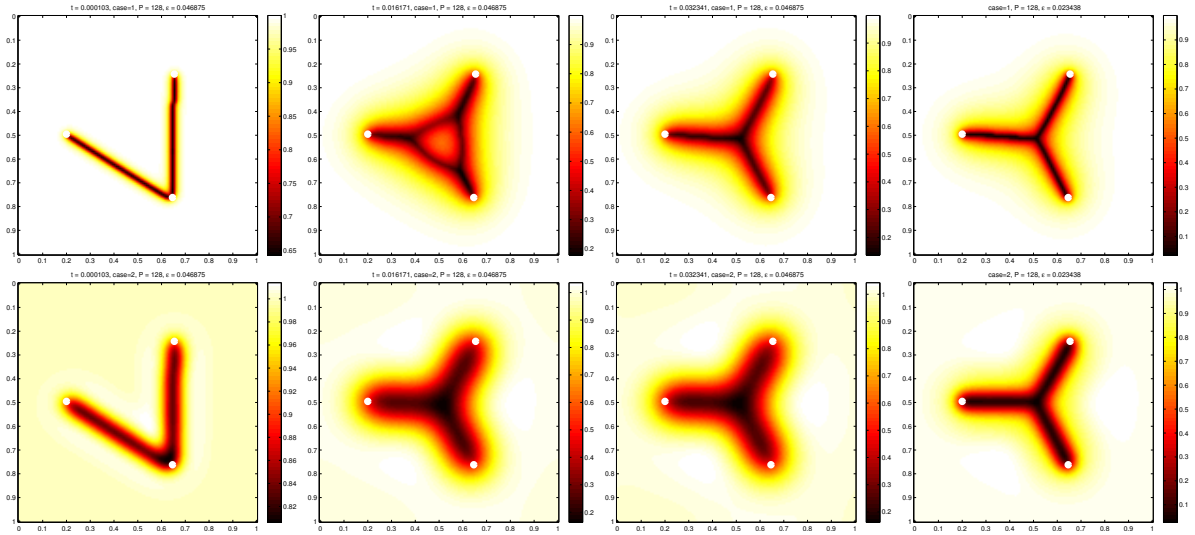

Figure 5: Example with 3 points with the set of parameters $P = 2^7$, $\varepsilon = 6/P$, $\delta_t = \varepsilon$ and $\lambda_\varepsilon = \varepsilon^2$. The first and second lines correspond respectively to the operators $-\varepsilon\Delta$ and $-\varepsilon^3\Delta^2$. From left to right: the phase field function u at different times t during the iterations. For the last picture, we plot the stationary solution obtained after dividing the ε parameter by 2.

3.4 Numerical comparison of the solution obtained with the geodesic terms R_ε and $\tilde{R}_{\varepsilon,\max}$

We recall that the geodesic terms R_ε and $\tilde{R}_{\varepsilon,\max}$ are respectively defined by

$$\tilde{R}_\varepsilon(u,\boldsymbol{\gamma}) = \frac{1}{\lambda_\varepsilon}\int_\Omega \omega^\varepsilon[\boldsymbol{\gamma}](\delta_\varepsilon + u^2)\,dx, \text{ with } \omega^\varepsilon[\boldsymbol{\gamma}] = \sum_{i=1}^{N}(\rho_{\varepsilon^\alpha} * \mathcal{H}^1|_{\Gamma(\gamma_i)}),$$

and by

$$\tilde{R}_{\varepsilon,\max} = \frac{1}{\lambda_\varepsilon}\int_\Omega \omega^\varepsilon_{\max}[\boldsymbol{\gamma}](\delta_\varepsilon + u^2)\,dx, \text{ with } \omega^\varepsilon_{\max}[\boldsymbol{\gamma}] = \mathrm{Max}_{i=1}^{N}\left\{\rho_{\varepsilon^\alpha} * \mathcal{H}^1|_{\Gamma(\gamma_i)}\right\}.$$

This section is motivated by the observation that the weight $\omega^\varepsilon[\boldsymbol{\gamma}]$ at point x depends on the number of geodesics that cross this point. Hence, this weight can be very sensitive to the number of endpoints a_i, which raises some numerical difficulties to fix the value of $\boldsymbol{\gamma}_\varepsilon$ in practice. To reduce these drawbacks, we propose to slightly modify this geodesic term, in such a way that the weight of the penalized term no longer depends on the number of geodesics going through the points. To this aim, we replace the sum

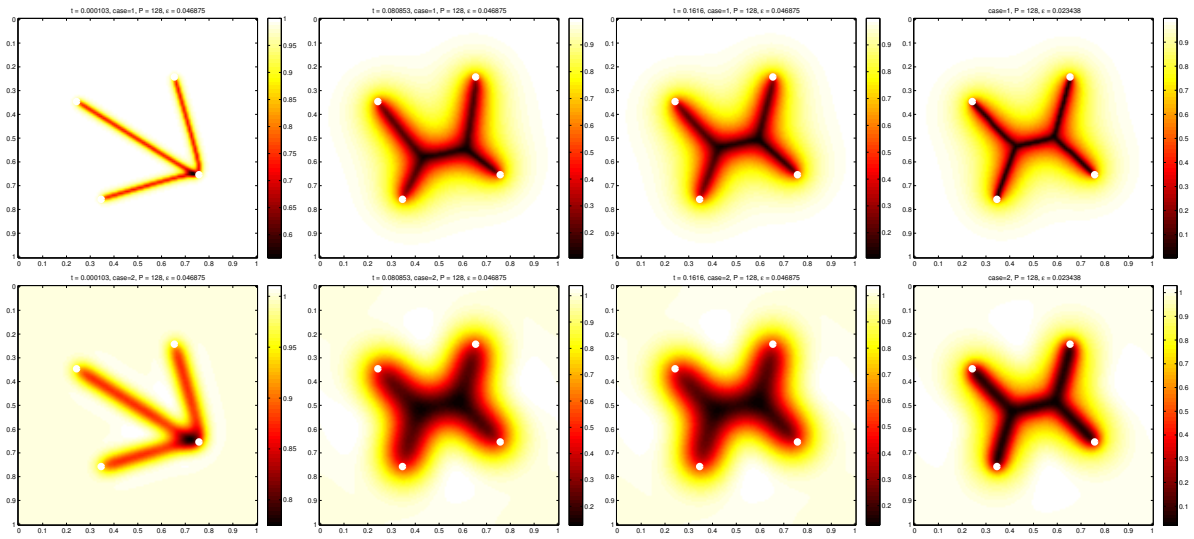

Figure 6: Example with 4 points with the set of parameters $P = 2^7$, $\varepsilon = 6/P$, $\delta_t = \varepsilon$ and $\lambda_\varepsilon = \varepsilon^2$. The first and the second lines correspond respectively to the operators $-\varepsilon\Delta$ and $-\varepsilon^3\Delta^2$. Left to right: the phase field function u at different times t during the iterations. In the last picture, we plot the stationary solution obtained after dividing the ε parameter by 2.

of the contributions of all the geodesics, by the maximum contribution. This yields the definition of the new weight $\omega^{\varepsilon}_{\max}[\boldsymbol{\gamma}]$ and the associated penalized term $\tilde{R}_{\varepsilon,\max}$.

In order to compare the two models, we present in Figures 8 and 9 the results obtained using the penalized terms $\tilde{R}_\varepsilon$ and $\tilde{R}_{\varepsilon,\max}$, and the same configurations of point a_i. In every simuation, we consider the set of parameters $P = 2^8$, $\delta_t = \varepsilon$ and $\lambda_\varepsilon = \varepsilon^2$. At the beginning of the iterations, ε is fixed to $12/P$ and the solution is computed until convergence to a stationary solution. Then, we divide ε by $\sqrt{2}$ and we iterate the process until $\varepsilon < 2/P$. In both figures, the first and the second lines correspond respectively to the model $\tilde{R}^{\mu}_{\varepsilon}$ and $\tilde{R}^{\mu}_{\varepsilon,\max}$, and each picture corresponds respectively to $\varepsilon = 6\sqrt{2}/P$, $\varepsilon = 6/P$, $\varepsilon = 3\sqrt{2}/P$, $\varepsilon = 3/P$ and $\varepsilon = (3/\sqrt{2})/P$. We can clearly observe that when $\tilde{R}^{\mu}_{\varepsilon}$ is used, the width of the diffuse interface depends on the number of points x_i, which is not the case with the new model $\tilde{R}^{\mu}_{\varepsilon,\max}$, that provides much cleaner solutions and is able to capture the geodesics more accurately.

3.5 Numerical experiments with a large number of points

We now test our numerical method to approximate the solution of the Steiner problem with a large number of points. In view of the numerical results presented in the previous paragraphs, we consider the phase field model

$$\overline{E}_\varepsilon(u, \boldsymbol{\gamma}) = \tilde{P}_\varepsilon(u) + \tilde{R}_{\varepsilon,\max}(u, \boldsymbol{\gamma}).$$

As previously, we compute the stationary solutions associated to different value of ε and the set of parameters is fixed to $P = 2^8$, $\delta_t = \varepsilon$ and $\lambda_\varepsilon = \varepsilon^2$. We present two numerical experiments in Figure 10, with respectively 50 and 100 points randomly distributed in the computation box Q. We observe a good behavior of the solution which becomes more precise as ε goes to 0. However, we can not guarantee

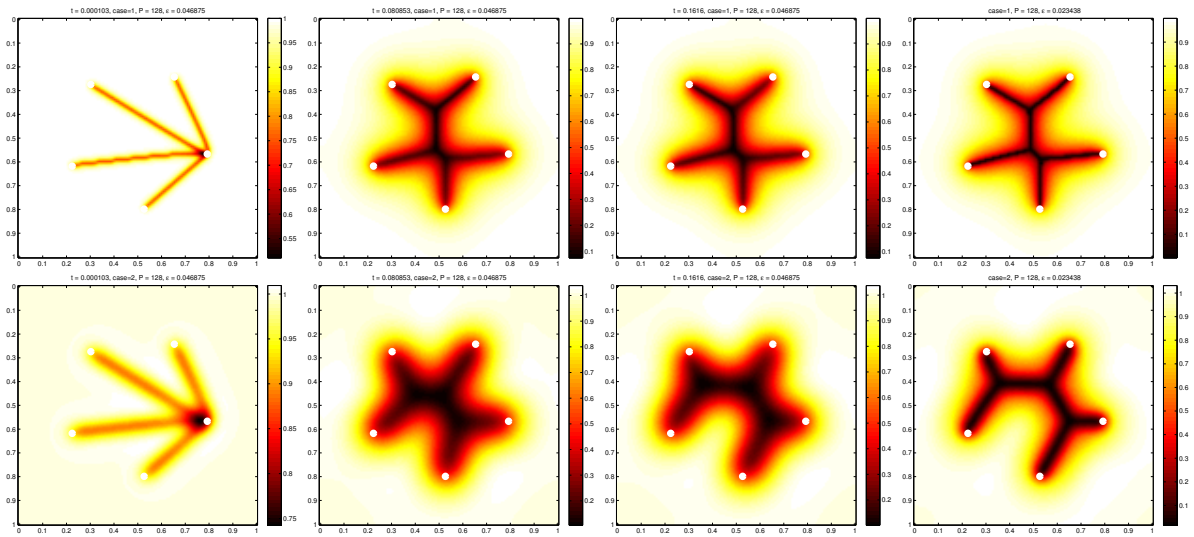

Figure 7: Example with 4 points with the set of parameters $P = 2^7$, $\varepsilon = 6/P$, $\delta_t = \varepsilon$ and $\lambda_\varepsilon = \varepsilon^2$. The first and the second line correspond respectively to the operator $\varepsilon\Delta$ and the operator $-\varepsilon^3\Delta^2$. Left to right : The phase field function u at different time t along the iteration. For the last picture, we plot the stationary solution after dividing the ε parameter by 2.

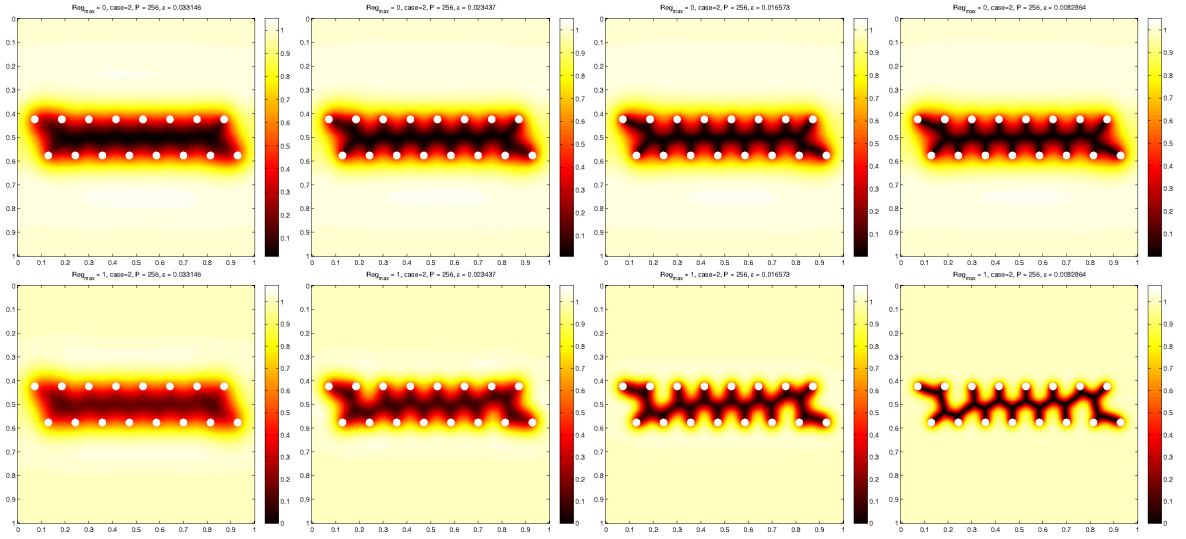

Figure 8: Numerical experiment with 16 points with the set of parameters $P = 2^8$, $\delta_t = \varepsilon$ and $\lambda_\varepsilon = \varepsilon^2$. The first and second line correspond respectively to the geodesic term R_ε, $\tilde{R}_{\varepsilon,\max}$. Left to right : stationary solution u^ε obtained respectively with different value of ε: $\varepsilon = 6\sqrt{2}/P$, $\varepsilon = 6/P$, $\varepsilon = 3\sqrt{2}/P$ and $\varepsilon = 3/P$.

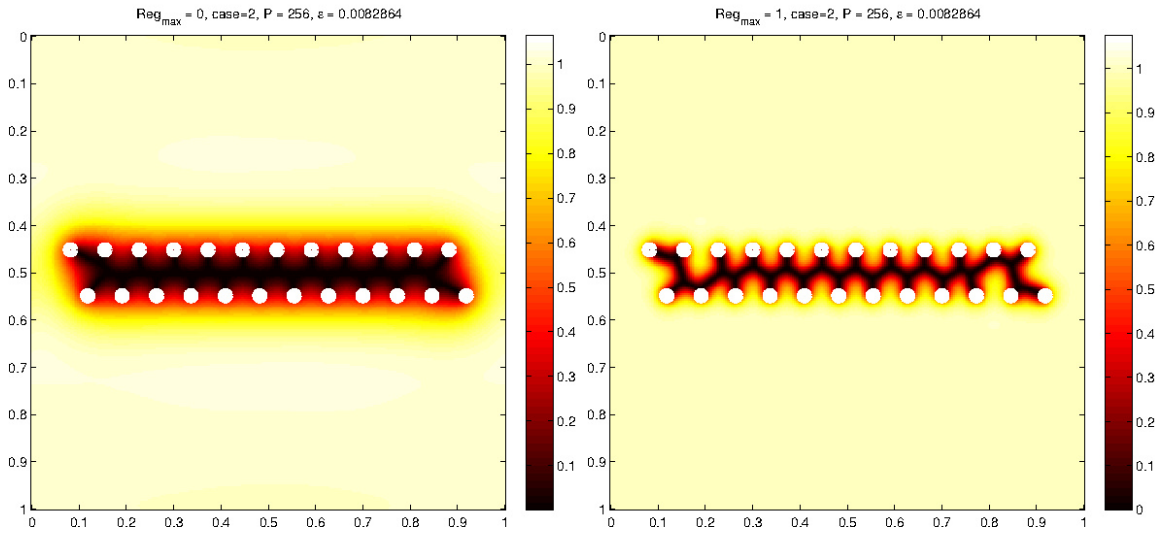

Figure 9: Numerical experiment with 24 points with the set of parameters $P = 2^8$, $\delta_t = \varepsilon$, $\lambda_\varepsilon = \varepsilon^2$. The left and the right picture correspond respectively to the stationary solution u^ε obtained with $\varepsilon = 3/P$ and using respectively the geodesic term R_ε and $\tilde{R}_{\varepsilon,\max}$.

that the iterations converge to a global minimizer of the Steiner problem; in particular, we can observe the presence of a cycle on the final solution obtained using 100 points, which means that this solution is clearly not optimal.

3.6 Numerical experiments in dimension 3

We finally propose to test our numerical method in the 3-dimensional case. More precisely, we consider the phase field energy

$$\overline{E}^{\mu}_{\varepsilon}(u, \boldsymbol{\gamma}) = \tilde{P}_\varepsilon(u) + \tilde{R}_{\varepsilon,\max}(u, \boldsymbol{\gamma}).$$

where $\tilde{P}_\varepsilon$ now satisfies

$$\tilde{P}_\varepsilon(u) = \int_Q \frac{\varepsilon^2}{2}(\Delta u)^2 + \frac{1}{\varepsilon^2} V(u)\, dx.$$

We plot in figure 11 the results of two first experiments that consider 3 and 10 points respectively. Each red ball represents a point a_i and the green surface corresponds to the level set $(1 + min(u))/2$ of u, defined as the boundary of the set $\{x \in Q; u(x) \leq (1 + min(u))/2\}$. The approximations of u are computed with the following set of parameters: $P = 2^7$, $\delta_t = \varepsilon^2$ and $\lambda_\varepsilon = \varepsilon^2$. More precisely, we compute u^n until we reach a stationary solution, and then divide ε by 2 and compute a new stationary solution.
Notice that the solution seems to converge to a global minimizer at least in the case of 3 points.

We conclude this section by a last example where the points a_i are located on the corners of a cube. This experiment is very sensitive since for reasons of symmetry, there exist many global minimizers, and

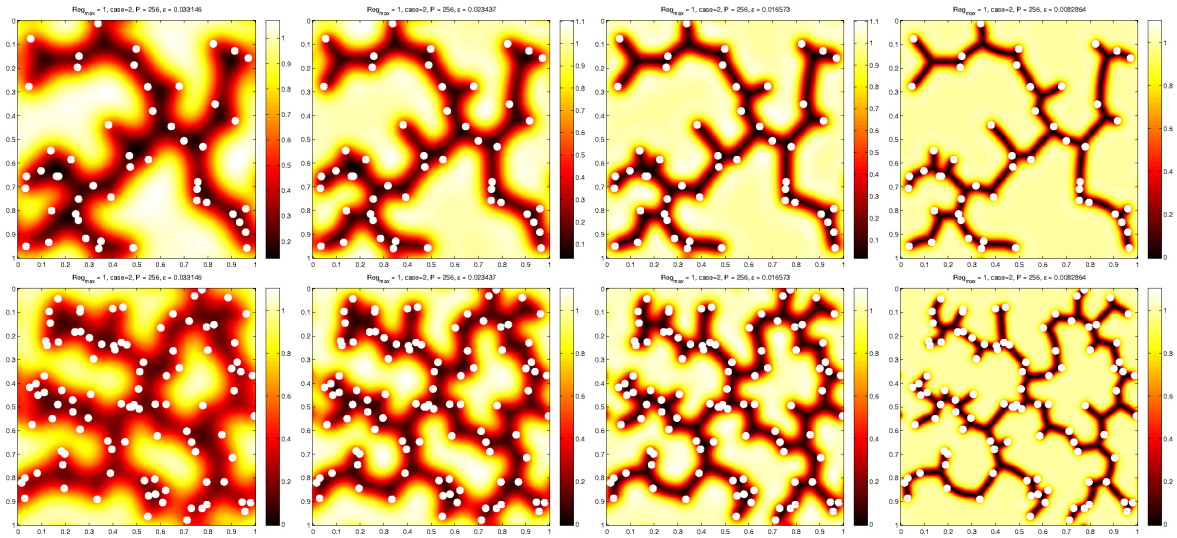

Figure 10: Numerical experiments with a large number of points, with the set of parameters $P = 2^8$, $\delta_t = \varepsilon$ and $\lambda_\varepsilon = \varepsilon^2$. The first and second lines correspond respectively to the case of 50 and 100 points randomly distributed in the computation box Q. Left to right: stationary solution u^ε obtained with different values of ε: $\varepsilon = 6\sqrt{2}/P$, $\varepsilon = 6/P$, $\varepsilon = 3\sqrt{2}/P$ and $\varepsilon = 3/P$.

consequently, a lot of local minimizers as well. Using the following set of parameter $P = 2^6$, $\delta_t = \varepsilon^2$ and $\lambda_\varepsilon = \epsilon^2$, we represent in figure 12 the evolution of u during the iterations and until convergence to a stationary solution. The last picture concerns the stationary solution obtained with $\varepsilon = 2.5/P$. We observe that the algorithm seems to converge to an approximation of a global minimizer, which highlights the great potential of the method also in dimension 3.

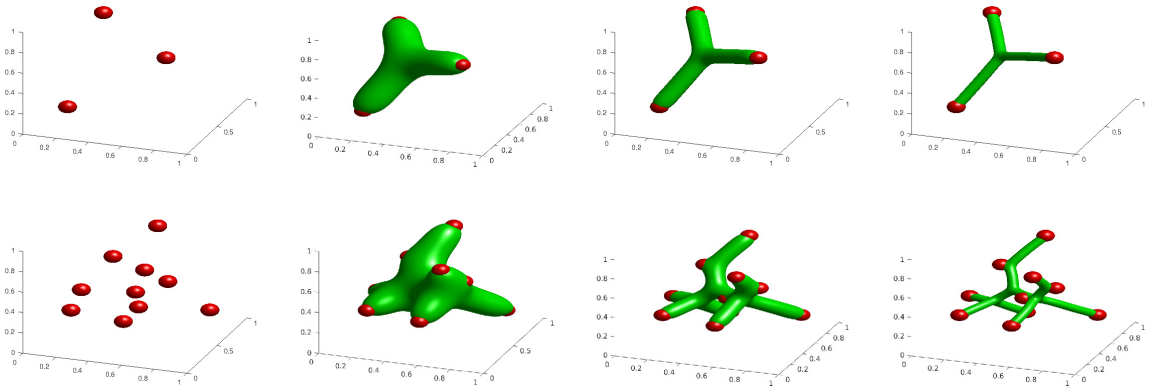

Figure 11: Numerical experiments in $3D$ with the set of parameters $P = 2^7$, $\delta_t = \varepsilon^2$ and $\lambda_\varepsilon = \varepsilon^2$. The first and second lines correspond respectively to the case of 3 and 10 points randomly distributed in the computation box Q. From left to right: initial red points a_i, stationary solution u^ε obtained with $\varepsilon = 8/P$, $\varepsilon = 4/P$ and with $\varepsilon = 2/P$.

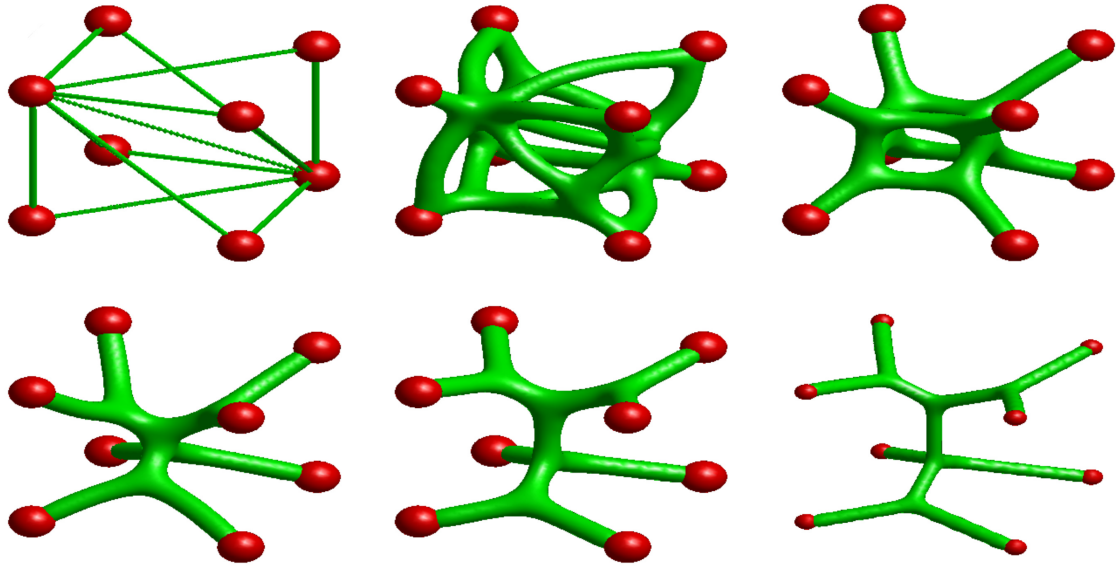

Figure 12: Numerical experiments in $3D$: the cube case with $P = 2^6$, $\delta_t = \varepsilon^2$ and $\lambda_\varepsilon = \varepsilon^2$ and $\varepsilon = 5/P$. Each pictures corresponds to the solution along the iterations until to converge to a stationary solution. The last picture picture corresponds to the stationary solution obtained with $\varepsilon = 2.5/P$.

References

[1] M. Abramowitz. *Handbook of Mathematical Functions, With Formulas, Graphs, and Mathematical Tables*. Dover Publications, Incorporated, 1974.

[2] F. Benmansour, G. Carlier, G. Peyré, and F. Santambrogio. Derivatives with Respect to Metrics and Applications: Subgradient Marching Algorithm. *Numerische Mathematik*, 116(3):357–381, 2010.

[3] M. Bonafini, G. Orlandi, and E. Oudet. Variational approximation of functionals defined on 1-dimensional connected sets: the planar case. *Preprint*, 2016.

[4] M. Bonnivard, A. Lemenant, and V. Millot. On a phase field approximation of the planar Steiner problem: existence, regularity, and asymptotic of minimizers. To appear in Interfaces and Free Boundaries, 2018.

[5] M. Bonnivard, A. Lemenant, and F. Santambrogio. Approximation of length minimization problems among compact connected sets. *SIAM Journal on Mathematical Analysis*, 47(2):1489–1529, 2015.

[6] M. Burger, T. Esposito, and C. I. Zeppieri. Second-order edge-penalization in the Ambrosio–Tortorelli functional. *Multiscale Modeling & Simulation*, 13(4):1354–1389, 2015.

[7] A. Chambolle, L. Ferrari, and B. Merlet. A phase-field approximation of the Steiner problem in dimension two. *Preprint*, 2017.

[8] A. Chambolle, L. Ferrari, and B. Merlet. Variational approximation of size-mass energies for k-dimensional currents. *Preprint*, 2017.

[9] V. L. do Forte, F. M. T Montenegro, J. A. M. Brito, and N. Maculan. Iterated local search algorithms for the Euclidean Steiner tree problem in n dimensions. *Int. Trans. Oper. Res.*, 23(6):1185–1199, 2016.

[10] D. Eyre. Computational and mathematical models of microstructural evolution. *Warrendale:The Material Research Society*, 1998.

[11] R. M. Karp. *Reducibility among Combinatorial Problems*, pages 85–103. Springer US, Boston, MA, 1972.

[12] A. Lemenant and F. Santambrogio. A Modica-Mortola approximation for the Steiner problem. *C. R. Math. Acad. Sci. Paris*, 352(5):451–454, 2014.

[13] E. Paolini and E. Stepanov. Existence and regularity results for the Steiner problem. *Calc. Var. Partial Differential Equations*, 46(3-4):837–860, 2013.

[14] J. A. Sethian. Fast marching methods. *SIAM Review*, 41(2):199–235, 1999.

[15] J. A. Sethian. *Level Set Methods and Fast Marching Methods*. Cambridge University Press, second edition edition, 1999.

[16] J. Shen, C. Wang, X. Wang, and S. M. Wise. Second-order convex splitting schemes for gradient flows with Ehrlich-Schwoebel type energy: Application to thin film epitaxy. *SIAM J. Numerical Analysis*, 50(1):105–125, 2012.